FIGURE 1.1. $f(u)$ and $f'(u)$ with $M = 2$.

Due to the possibility of the existence of shocks in the solution of the hyperbolic conservation laws (1.1), the weak solutions are sought. The function $u \in L^\infty(Q)$ is called a weak solution of the conservation laws (1.1) if

$$\int_Q \left\{ u \frac{\partial \phi}{\partial t} + f(u) \frac{\partial \phi}{\partial x} \right\} = 0 \quad \text{for all } \phi \in C_0^\infty(Q).$$

15 Notice that the weak solution is not unique. Among the weak solutions, the entropy
 16 solution is physically relevant and unique. The weak solution that satisfies Oleinik
 17 entropy condition [19]

$$(1.3) \quad \frac{f(u) - f(u_l)}{u - u_l} \geq s \geq \frac{f(u) - f(u_r)}{u - u_r} \quad \text{for all } u \text{ between } u_l \text{ and } u_r$$

18 is the entropy solution, where u_l , u_r are the function values to the left and right
 19 of the shock respectively, and the shock speed s satisfies Rankine-Hugoniot jump
 20 condition [17, 10]

$$(1.4) \quad s = \frac{f(u_l) - f(u_r)}{u_l - u_r}.$$

21 The classical BL equation (1.1) with flux function $f(u)$ as given in (1.2) has been
 22 well studied (see [14] for an introduction). Let α be the solution of $f'(u) = \frac{f(u)}{u}$,
 23 i.e.,

$$(1.5) \quad \alpha = \sqrt{\frac{M}{M+1}}.$$

24 The entropy solution of the classical BL equation can be classified into two cate-
 25 gories:

- 26 (1) If $0 < u_B \leq \alpha$, the entropy solution has a single shock at $\frac{x}{t} = \frac{f(u_B)}{u_B}$.
 27 (2) If $\alpha < u_B < 1$, the entropy solution contains a rarefaction between u_B and
 28 α for $f'(u_B) < \frac{x}{t} < f'(\alpha)$ and a shock at $\frac{x}{t} = \frac{f(\alpha)}{\alpha}$.

29 These two types of solutions are shown in Figure 1.2 for $M = 2$. In either case,
 30 the entropy solution of the classical BL equation (1.1) is a non-increasing function
 31 of x at any given time $t > 0$. However, the experiments of two-phase flow in
 32 porous medium reveal complex infiltration profiles, which may involve overshoot,
 33 i.e., profiles may not be monotone [7]. This suggests the need of modification to
 34 the classical BL equation (1.1).

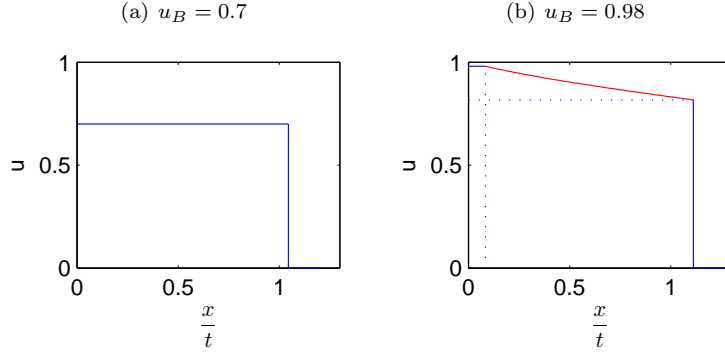


FIGURE 1.2. The entropy solution of the classical BL equation ($M = 2$, $\alpha = \sqrt{\frac{2}{3}} \approx 0.8165$). (a) $0 < u_B = 0.7 \leq \alpha$, the solution consists of one shock at $\frac{x}{t} = \frac{f(u_B)}{u_B}$; (b) $\alpha < u_B = 0.98 < 1$, the solution consists of a rarefaction between u_B and α for $f'(u_B) < \frac{x}{t} < f'(\alpha)$ and a shock at $\frac{x}{t} = \frac{f(\alpha)}{\alpha}$.

35 To better describe the infiltration profiles, we go back to the origins of (1.1).
 36 Let S_i be the saturation of water/oil ($i = w, o$) and assume that the medium is
 37 completely saturated, i.e. $S_w + S_o = 1$. The conservation of mass gives

$$(1.6) \quad \phi \frac{\partial S_i}{\partial t} + \frac{\partial q_i}{\partial x} = 0$$

38 where ϕ is the porosity of the medium (relative volume occupied by the pores) and
 39 q_i denotes the discharge of water/oil with $q_w + q_o = q$, which is assumed to be a
 40 constant in space due to the complete saturation assumption. Throughout of this
 41 work, we consider it constant in time as well. By Darcy's law

$$(1.7) \quad q_i = -k \frac{k_{r_i}(S_i)}{\mu_i} \frac{\partial P_i}{\partial x}, \quad i = w, o$$

42 where k denotes the absolute permeability, k_{r_i} is the relative permeability and μ_i
 43 is the viscosity of water/oil. Instead of considering constant capillary pressure as
 44 adopted by the classical BL equation (1.1), Hassanizadeh and Gray [8, 9] have
 45 defined the dynamic capillary pressure as

$$(1.8) \quad P_c = P_o - P_w = p_c(S_w) - \phi \tau \frac{\partial S_w}{\partial t}$$

46 where $p_c(S_w)$ is the *static* capillary pressure and τ is a positive constant, and $\frac{\partial S_w}{\partial t}$
 47 is the dynamic effects. Using Corey [6, 20] expressions with exponent 2, $k_{r_w}(S_w) =$
 48 S_w^2 , $k_{r_o}(S_o) = S_o^2$, rescaling $x \frac{\phi}{q} \rightarrow x$ and combining (1.6)-(1.8), the single equation
 49 for the water saturation $u = S_w$ is

$$(1.9) \quad \frac{\partial u}{\partial t} + \frac{\partial}{\partial x} \left[\frac{u^2}{u^2 + M(1-u)^2} \right] = - \frac{\partial}{\partial x} \left[\frac{\phi^2}{q^2} \frac{k(1-u)^2 u^2}{\mu_w(1-u)^2 + \mu_o u^2} \frac{\partial}{\partial x} \left(\frac{p_c(u)}{\phi} - \tau \frac{\partial u}{\partial t} \right) \right]$$

50 where $M = \frac{\mu_w}{\mu_o}$ [22]. Linearizing the right hand side of (1.9) and rescaling the
 51 equation as in [21, 20], the modified Buckley-Leverett equation (MBL) is derived

52 as

$$(1.10) \quad \frac{\partial u}{\partial t} + \frac{\partial f(u)}{\partial x} = \epsilon \frac{\partial^2 u}{\partial x^2} + \epsilon^2 \tau \frac{\partial^3 u}{\partial x^2 \partial t}$$

53 where the water fractional flow function $f(u)$ is given as in (1.2). Notice that, if P_c
 54 in (1.8) is taken to be constant, then (1.9) gives the classical BL equation; while
 55 if the dispersive parameter τ is taken to be zero, then (1.10) gives the viscous BL
 56 equation, which still displays monotone water saturation profile. Thus, in addition
 57 to the classical second order viscous term ϵu_{xx} , the MBL equation (1.10) is
 58 an extension involving a third order mixed derivative term $\epsilon^2 \tau u_{xxt}$. Van Duijn et
 59 al. [21] showed that the value τ is critical in determining the type of the solution
 60 profile. In particular, for certain Riemann problems, the solution profile of (1.10)
 61 is not monotone when τ is larger than the threshold value τ_* , where τ_* was numerically
 62 determined to be 0.61 [21]. The non-monotonicity of the solution profile is
 63 consistent with the experimental observations [7].

64 The classical BL equation (1.1) is hyperbolic, and the numerical schemes for
 65 hyperbolic equations have been well developed (e.g. [14, 15, 4, 5, 18, 12]). The
 66 MBL equation (1.10), however, is pseudo-parabolic, we will illustrate how to extend
 67 the central schemes [18, 12, 13] to solve (1.10) numerically. Unlike the finite domain
 68 of dependence for the classical BL equation (1.1), the domain of dependence for
 69 the MBL equation (1.10) is infinite. This naturally raises the question for the
 70 choice of computational domain. To answer this question, we will first study the
 71 MBL equation equipped with two types of domains and corresponding boundary
 72 conditions. One is the half line boundary value problem

$$(1.11) \quad \begin{aligned} u_t + (f(u))_x &= \epsilon u_{xx} + \epsilon^2 \tau u_{xxt} & \text{in} & \quad Q = \{(x, t) : x > 0, t > 0\} \\ u(x, 0) &= u_0(x) & & \quad x \in [0, \infty) \\ u(0, t) &= g_u(t), \quad \lim_{x \rightarrow \infty} u(x, t) = 0 & & \quad t \in [0, \infty) \\ u_0(0) &= g_u(0) & & \quad \text{compatibility condition} \end{aligned}$$

73 and the other one is finite interval boundary value problem

$$(1.12) \quad \begin{aligned} v_t + (f(v))_x &= \epsilon v_{xx} + \epsilon^2 \tau v_{xxt} & \text{in} & \quad \tilde{Q} = \{(x, t) : x \in (0, L), t > 0\} \\ v(x, 0) &= v_0(x) & & \quad x \in [0, L] \\ v(0, t) &= g_v(t), \quad v(L, t) = h(t) & & \quad t \in [0, \infty) \\ v_0(0) &= g_v(0), \quad v_0(L) = h(0) & & \quad \text{compatibility condition.} \end{aligned}$$

74 Considering

$$(1.13) \quad u_0(x) = \begin{cases} v_0(x) & \text{for } x \in [0, L] \\ 0 & \text{for } x \in [L, +\infty) \end{cases}, \quad g_u(t) = g_v(t) \equiv g(t), \quad h(t) \equiv 0,$$

75 we will show the relation between the solutions of problems (1.11) and (1.12). To
 76 the best knowledge of the authors, there is no such study for MBL equation (1.10).
 77 Similar questions were answered for BBM equation [1, 2].

78 The organization of this paper is as follows. Section 2 will bring forward the
 79 exact theory comparing the solutions of (1.11) and (1.12). The difference between
 80 the solutions of these two types of problems decays exponentially with respect to
 81 the length of the interval L for practically interesting initial profiles. This provides
 82 a theoretical justification for the choice of the computational domain. In section

3, high order central schemes will be developed for MBL equation in finite interval domain. We provide a detailed derivation on how to extend the central schemes [18, 12] for conservation laws to solve the MBL equation (1.10). The idea of adopting numerical schemes originally designed for hyperbolic equations to pseudo-parabolic equations is not restricted to central type schemes only ([23, 24]). The numerical results in section 4 show that the water saturation profile strongly depends on the dispersive parameter τ value as studied in [21]. For $\tau > \tau_*$, the MBL equation (1.10) gives non-monotone water saturation profiles for certain Riemann problems as suggested by experimental observations [7]. Section 5 gives the conclusion of the paper and the possible future directions.

2. THE HALF LINE PROBLEM VERSUS THE FINITE INTERVAL PROBLEM

Let $u(x, t)$ be the solution to the half line problem (1.11), and let $v(x, t)$ be the solution to the finite interval problem (1.12). We consider the natural assumptions (1.13). The goal of this section is to develop an estimate of the difference between u and v on the spatial interval $[0, L]$ at a given finite time t . The main result of this section is

Theorem 2.1 (The main Theorem). *If $u_0(x)$ satisfies*

$$(2.1) \quad u_0(x) = \begin{cases} C_u & x \in [0, L_0] \\ 0 & x > L_0 \end{cases}$$

where $L_0 < L$ and C_u , are positive constants, then

$$\|u(\cdot, t) - v(\cdot, t)\|_{H_{L, \epsilon, \tau}^1} \leq D_{1; \epsilon, \tau}(t) e^{-\frac{\lambda L}{\epsilon \sqrt{\tau}}} + D_{2; \epsilon, \tau}(t) e^{-\frac{\lambda(L-L_0)}{\epsilon \sqrt{\tau}}}$$

for some $0 < \lambda < 1$, $D_{1; \epsilon, \tau}(t) > 0$ and $D_{2; \epsilon, \tau}(t) > 0$, where

$$\|Y(\cdot, t)\|_{H_{L, \epsilon, \tau}^1} := \sqrt{\int_0^L Y(x, t)^2 + (\epsilon \sqrt{\tau} Y_x(x, t))^2 dx}$$

100

Notice that the initial condition (2.1) we considered is the Riemann problem. Theorem 2.1 shows that the solution to the half line problem (1.11) can be approximated as accurately as one wants by the solution to the finite interval problem (1.12) in the sense that $D_{1; \epsilon, \tau}(t)$, $D_{2; \epsilon, \tau}(t)$, $\frac{\lambda L}{\epsilon \sqrt{\tau}}$ and $\frac{\lambda(L-L_0)}{\epsilon \sqrt{\tau}}$ can be controlled.

To prove theorem 2.1, we first derive the implicit solution formulae for the half line problem and the finite interval problem in section 2.1 and section 2.2 respectively. The implicit solution formulae are in integral form, which are derived by separating the x -derivative from the t -derivative, and formally solving a first order linear ODE in t and a second order non-homogeneous ODE in x . In section 2.3, we use Gronwall's inequality multiple times to obtain the desired result in theorem 2.1.

2.1. Half line problem. In this section, we derive the implicit solution formula for the half line problem (1.11) (with $g_u(t) = g(t)$). To solve (1.11), we first rewrite (1.11) by separating the x -derivative from the t -derivative,

$$(2.2) \quad \left(I - \epsilon^2 \tau \frac{\partial^2}{\partial x^2} \right) \left(u_t + \frac{1}{\epsilon \tau} u \right) = \frac{1}{\epsilon \tau} u - (f(u))_x.$$

115 By using integrating factor method, we formally integrate (2.2) over $[0, t]$ to obtain
 116

$$(2.3) \quad \left(I - \epsilon^2 \tau \frac{\partial^2}{\partial x^2} \right) \left(u - e^{-\frac{t}{\epsilon\tau}} u_0 \right) = \int_0^t \left(\frac{1}{\epsilon\tau} u - (f(u))_x \right) e^{-\frac{t-s}{\epsilon\tau}} ds.$$

117 Furthermore, we let

$$(2.4) \quad A = u - e^{-\frac{t}{\epsilon\tau}} u_0,$$

118 then (2.3) can be written as

$$(2.5) \quad A'' - \frac{1}{\epsilon^2 \tau} A = \int_0^t \left(-\frac{1}{\epsilon^3 \tau^2} u + \frac{1}{\epsilon^2 \tau} (f(u))_x \right) e^{-\frac{t-s}{\epsilon\tau}} ds, \quad \text{where } ' = \frac{\partial}{\partial x}.$$

119 Notice that (2.5) is a second-order non-homogeneous ODE in x -variable along with
 120 the boundary conditions

$$(2.6) \quad \begin{aligned} A(0, t) &= u(0, t) - e^{-\frac{t}{\epsilon\tau}} u_0(0) = g(t) - e^{-\frac{t}{\epsilon\tau}} g(0), \\ A(\infty, t) &= u(\infty, t) - e^{-\frac{t}{\epsilon\tau}} u_0(\infty) = 0. \end{aligned}$$

121 To solve (2.5), we first solve the corresponding linear homogeneous equation with
 122 the non-zero boundary conditions (2.6). We then find a particular solution for the
 123 non-homogeneous equation with zero boundary conditions by introducing a Green's
 124 function $G(x, \xi)$ and a kernel $K(x, \xi)$ for the non-homogeneous terms u and $(f(u))_x$
 125 respectively. Combining the solutions for the two non-homogeneous terms and the
 126 homogeneous part with boundary conditions, we get the solution for equation (2.5)
 127 satisfying the boundary conditions (2.6):

$$(2.7) \quad \begin{aligned} A(x, t) &= -\frac{1}{\epsilon^3 \tau^2} \int_0^t \int_0^{+\infty} G(x, \xi) u(\xi, s) e^{-\frac{t-s}{\epsilon\tau}} d\xi ds \\ &+ \frac{1}{\epsilon^2 \tau} \int_0^t \int_0^{+\infty} K(x, \xi) f(u) e^{-\frac{t-s}{\epsilon\tau}} d\xi ds \\ &+ \left(g(t) - e^{-\frac{t}{\epsilon\tau}} g(0) \right) e^{-\frac{x}{\epsilon\sqrt{\tau}}} \end{aligned}$$

128 where the Green's function $G(x, \xi)$ and the kernel $K(x, \xi)$ are

$$(2.8) \quad G(x, \xi) = \frac{\epsilon\sqrt{\tau}}{2} \left(e^{-\frac{x+\xi}{\epsilon\sqrt{\tau}}} - e^{-\frac{|x-\xi|}{\epsilon\sqrt{\tau}}} \right),$$

$$(2.9) \quad K(x, \xi) = -\frac{\partial G(x, \xi)}{\partial \xi} = \frac{1}{2} \left(e^{-\frac{x+\xi}{\epsilon\sqrt{\tau}}} + \operatorname{sgn}(x - \xi) e^{-\frac{|x-\xi|}{\epsilon\sqrt{\tau}}} \right).$$

129 To recover the solution for the half line problem (1.11), we refer to the definition of
 130 A in (2.4). Thus, the implicit solution formula for the half line problem (1.11) is

$$(2.10) \quad \begin{aligned} u(x, t) &= -\frac{1}{2\epsilon^2 \tau \sqrt{\tau}} \int_0^t \int_0^{+\infty} \left(e^{-\frac{x+\xi}{\epsilon\sqrt{\tau}}} - e^{-\frac{|x-\xi|}{\epsilon\sqrt{\tau}}} \right) u(\xi, s) e^{-\frac{t-s}{\epsilon\tau}} d\xi ds \\ &+ \frac{1}{2\epsilon^2 \tau} \int_0^t \int_0^{+\infty} \left(e^{-\frac{x+\xi}{\epsilon\sqrt{\tau}}} + \operatorname{sgn}(x - \xi) e^{-\frac{|x-\xi|}{\epsilon\sqrt{\tau}}} \right) f(u) e^{-\frac{t-s}{\epsilon\tau}} d\xi ds \\ &+ \left(g(t) - e^{-\frac{t}{\epsilon\tau}} g(0) \right) e^{-\frac{x}{\epsilon\sqrt{\tau}}} + e^{-\frac{t}{\epsilon\tau}} u_0(x). \end{aligned}$$

131 **2.2. Finite interval problem.** The implicit solution for the finite interval problem
 132 (1.12) (with $g_v(t) = g(t)$) can be solved in a similar way. The only difference is that
 133 the additional boundary condition $h(t)$ at $x = L$ in (1.12) gives different boundary
 134 conditions for the non-homogeneous ODE in x -variable. Denote

$$(2.11) \quad A^L = v - e^{-\frac{t}{\epsilon\tau}} v_0,$$

135 then it satisfies

$$(2.12) \quad (A^L)'' - \frac{1}{\epsilon^2\tau} A^L = \int_0^t \left(-\frac{1}{\epsilon^3\tau^2} v + \frac{1}{\epsilon^2\tau} (f(v))_x \right) e^{-\frac{t-s}{\epsilon\tau}} ds \quad \text{where } ' = \frac{\partial}{\partial x}$$

with the boundary conditions

$$\begin{aligned} A^L(0, t) &= v(0, t) - e^{-\frac{t}{\epsilon\tau}} v_0(0) = g(t) - e^{-\frac{t}{\epsilon\tau}} g(0), \\ A^L(L, t) &= v(L, t) - e^{-\frac{t}{\epsilon\tau}} v_0(L) = h(t) - e^{-\frac{t}{\epsilon\tau}} h(0). \end{aligned}$$

136 These boundary conditions affect both the homogeneous solution and the partic-
 137 ular solution of (2.12) as follows

$$(2.13) \quad \begin{aligned} A^L(x, t) &= -\frac{1}{\epsilon^3\tau^2} \int_0^t \int_0^L G^L(x, \xi) v(\xi, s) e^{-\frac{t-s}{\epsilon\tau}} d\xi ds \\ &\quad + \frac{1}{\epsilon^2\tau} \int_0^t \int_0^L K^L(x, \xi) f(v) e^{-\frac{t-s}{\epsilon\tau}} d\xi ds \\ &\quad + c_1(t)\phi_1(x) + c_2(t)\phi_2(x) \end{aligned}$$

138 where the Green's function $G^L(x, \xi)$, the kernel $K^L(x, \xi)$ and the bases for the
 139 homogeneous solutions are

$$(2.14) \quad G^L(x, \xi) = \frac{\epsilon\sqrt{\tau}}{2(e^{\frac{2L}{\epsilon\sqrt{\tau}}} - 1)} \left(e^{\frac{x+\xi}{\epsilon\sqrt{\tau}}} + e^{\frac{2L-(x+\xi)}{\epsilon\sqrt{\tau}}} - e^{\frac{|x-\xi|}{\epsilon\sqrt{\tau}}} - e^{\frac{2L-|x-\xi|}{\epsilon\sqrt{\tau}}} \right),$$

140

$$(2.15) \quad \begin{aligned} K^L(x, \xi) &= -\frac{1}{2(e^{\frac{2L}{\epsilon\sqrt{\tau}}} - 1)} \left(e^{\frac{x+\xi}{\epsilon\sqrt{\tau}}} - e^{\frac{2L-(x+\xi)}{\epsilon\sqrt{\tau}}} \right. \\ &\quad \left. + \operatorname{sgn}(x - \xi) e^{\frac{|x-\xi|}{\epsilon\sqrt{\tau}}} - \operatorname{sgn}(x - \xi) e^{\frac{2L-|x-\xi|}{\epsilon\sqrt{\tau}}} \right), \end{aligned}$$

$$(2.16) \quad c_1(t) = g(t) - e^{-\frac{t}{\epsilon\tau}} g(0), \quad c_2(t) = h(t) - e^{-\frac{t}{\epsilon\tau}} h(0),$$

$$(2.17) \quad \phi_1(x) = \frac{e^{\frac{L-x}{\epsilon\sqrt{\tau}}} - e^{\frac{-L+x}{\epsilon\sqrt{\tau}}}}{e^{\frac{L}{\epsilon\sqrt{\tau}}} - e^{\frac{-L}{\epsilon\sqrt{\tau}}}}, \quad \text{and} \quad \phi_2(x) = \frac{e^{\frac{x}{\epsilon\sqrt{\tau}}} - e^{\frac{-x}{\epsilon\sqrt{\tau}}}}{e^{\frac{L}{\epsilon\sqrt{\tau}}} - e^{\frac{-L}{\epsilon\sqrt{\tau}}}}.$$

141 Thus, the implicit solution formula for the finite interval problem (1.12) is

$$(2.18) \quad \begin{aligned} v(x, t) &= -\frac{1}{2\epsilon^2\tau\sqrt{\tau}(e^{\frac{2L}{\epsilon\sqrt{\tau}}} - 1)} \int_0^t \int_0^L \left(e^{\frac{x+\xi}{\epsilon\sqrt{\tau}}} + e^{\frac{2L-(x+\xi)}{\epsilon\sqrt{\tau}}} - e^{\frac{|x-\xi|}{\epsilon\sqrt{\tau}}} \right. \\ &\quad \left. - e^{\frac{2L-|x-\xi|}{\epsilon\sqrt{\tau}}} \right) v(\xi, s) e^{-\frac{t-s}{\epsilon\tau}} d\xi ds \\ &\quad - \frac{1}{2\epsilon^2\tau(e^{\frac{2L}{\epsilon\sqrt{\tau}}} - 1)} \int_0^t \int_0^L \left(e^{\frac{x+\xi}{\epsilon\sqrt{\tau}}} - e^{\frac{2L-(x+\xi)}{\epsilon\sqrt{\tau}}} + \operatorname{sgn}(x - \xi) e^{\frac{|x-\xi|}{\epsilon\sqrt{\tau}}} \right. \\ &\quad \left. - \operatorname{sgn}(x - \xi) e^{\frac{2L-|x-\xi|}{\epsilon\sqrt{\tau}}} \right) f(v) e^{-\frac{t-s}{\epsilon\tau}} d\xi ds \\ &\quad + c_1(t)\phi_1(x) + c_2(t)\phi_2(x) + e^{-\frac{t}{\epsilon\tau}} v_0(x). \end{aligned}$$

142 **2.3. Comparisons.** In this section, we will prove that the solution $u(x, t)$ to the
 143 half line problem can be approximated as accurately as one wants by the solution
 144 $v(x, t)$ to the finite interval problem as stated in Theorem 2.1.

145 Due to the difference in the integration domains, we do not use (2.10) and (2.18)
 146 directly for the comparison. Instead, we decompose $u(x, t)$ ($v(x, t)$ respectively)
 147 into two parts: $U(x, t)$ and $u_L(x, t)$ ($V(x, t)$ and $v_L(x, t)$ respectively), such that
 148 $U(x, t)$ ($V(x, t)$ respectively) enjoys zero initial condition and boundary conditions
 149 at $x = 0$ and $x = L$. We estimate the difference between $u(\cdot, t)$ and $v(\cdot, t)$ by
 150 estimating the differences between $u_L(\cdot, t)$ and $v_L(\cdot, t)$, $U(\cdot, t)$ and $V(\cdot, t)$, then
 151 applying the triangle inequality.

152

2.3.1. *Definitions and lemmas.* To assist the proof of Theorem 2.1 in section 2.3.3,
 we introduce some new notations in this section. We first decompose $u(x, t)$ as sum
 of two terms $U(x, t)$ and $u_L(x, t)$, such that

$$u(x, t) = U(x, t) + u_L(x, t) \quad x \in [0, +\infty)$$

153 where

$$(2.19) \quad u_L = e^{-\frac{t}{\epsilon\tau}} u_0(x) + c_1(t) e^{-\frac{x}{\epsilon\sqrt{\tau}}} + \left(u(L, t) - c_1(t) e^{-\frac{L}{\epsilon\sqrt{\tau}}} - e^{-\frac{t}{\epsilon\tau}} u_0(L) \right) \phi_2(x)$$

154 and $c_1(t)$ and $\phi_2(x)$ are given in (2.16) and (2.17) respectively. With this definition,
 155 u_L takes care of the initial condition $u_0(x)$ and boundary conditions $g(t)$ at $x = 0$
 156 and $x = L$ for $u(x, t)$. Then U satisfies an equation slightly different from the
 157 equation u satisfies in (1.11):

$$(2.20) \quad \begin{aligned} U_t - \epsilon U_{xx} - \epsilon^2 \tau U_{xxt} &= (u_t - \epsilon u_{xx} - \epsilon^2 \tau u_{xxt}) - ((u_L)_t - \epsilon (u_L)_{xx} - \epsilon^2 \tau (u_L)_{xxt}) \\ &= -(f(u))_x + \frac{1}{\epsilon\tau} u_L(x, t) \end{aligned}$$

158 In addition, $U(x, t)$ has zero initial condition and boundary conditions at $x = 0$
 159 and $x = L$, i.e.,

$$(2.21) \quad U(x, 0) = 0, \quad U(0, t) = 0, \quad U(L, t) = 0.$$

Similarly, for $v(x, t)$, let

$$v(x, t) = V(x, t) + v_L(x, t) \quad x \in [0, L]$$

160 where

$$(2.22) \quad v_L = e^{-\frac{t}{\epsilon\tau}} v_0(x) + c_1(t) \phi_1(x) + c_2(t) \phi_2(x)$$

161 and $c_1(t)$, $c_2(t)$ and $\phi_1(x)$, $\phi_2(x)$ are given in (2.16) and (2.17) respectively. With
 162 this definition, v_L takes care of the initial condition $v_0(x)$ and boundary conditions
 163 $g(t)$ and $h(t)$ at $x = 0$ and $x = L$ for $v(x, t)$. Then V satisfies an equation slightly
 164 different from the equation v satisfies in (1.12):

$$(2.23) \quad V_t - \epsilon V_{xx} - \epsilon^2 \tau V_{xxt} = -(f(v))_x + \frac{1}{\epsilon\tau} v_L(x, t)$$

165 with

$$(2.24) \quad V(x, 0) = 0, \quad V(0, t) = 0, \quad V(L, t) = 0.$$

Since, in the end, we want to study the difference between $U(x, t)$ and $V(x, t)$, we define

$$W(x, t) = V(x, t) - U(x, t) \quad \text{for} \quad x \in [0, L].$$

166 Because of (2.20) and (2.23), we have

$$(2.25) \quad W_t - \epsilon W_{xx} - \epsilon^2 \tau W_{xxt} = -(f(v) - f(u))_x + \frac{1}{\epsilon \tau} (v_L - u_L).$$

167 In lieu of (2.21) and (2.24), $W(x, t)$ also has zero initial condition and boundary
168 conditions at $x = 0$ and $x = L$, i.e.,

$$(2.26) \quad W(x, 0) = 0, \quad W(0, t) = 0, \quad W(L, t) = 0.$$

169 Now, to estimate $\|u - v\|$, we can estimate $\|W\| = \|V - U\|$ and estimate
170 $\|u_L - v_L\|$ separately. These estimates are done in section 2.3.3.

171 Next, we state the lemmas needed in the proof of Theorem 2.1. The proof of the
172 lemmas can be found in the appendix A and [22]. In all the lemmas, we assume
173 $0 < \lambda < 1$ and $u_0(x)$ satisfies

$$(2.27) \quad u_0(x) = \begin{cases} C_u & x \in [0, L_0] \\ 0 & x > L_0 \end{cases}$$

174 where $L_0 < L$ and C_u are positive constants. Notice that the constraint $\lambda \in (0, 1)$
175 is crucial in Lemmas 2.3, 2.4.

176 **Lemma 2.2.** $f(u) = \frac{u^2}{u^2 + M(1-u)^2} \leq Du$ where $D = \frac{f(\alpha)}{\alpha}$ and $\alpha = \sqrt{\frac{M}{M+1}}$.

177 **Lemma 2.3.** (i) $\int_0^{+\infty} \left| e^{-\frac{x+\xi}{\epsilon\sqrt{\tau}}} - e^{-\frac{|x-\xi|}{\epsilon\sqrt{\tau}}} \right| e^{\frac{\lambda x - \lambda \xi}{\epsilon\sqrt{\tau}}} d\xi \leq \frac{2\epsilon\sqrt{\tau}}{1-\lambda^2}$.

178 (ii) $\int_0^{+\infty} \left| e^{-\frac{x+\xi}{\epsilon\sqrt{\tau}}} - e^{-\frac{|x-\xi|}{\epsilon\sqrt{\tau}}} \right| e^{\frac{\lambda x - \xi}{\epsilon\sqrt{\tau}}} d\xi \leq \frac{\epsilon\sqrt{\tau}}{e(1-\lambda)}$.

179 (iii) $\int_0^{+\infty} \left| e^{-\frac{x+\xi}{\epsilon\sqrt{\tau}}} - e^{-\frac{|x-\xi|}{\epsilon\sqrt{\tau}}} \right| e^{\frac{\lambda x}{\epsilon\sqrt{\tau}}} |u_0(\xi)| d\xi \leq 2C_u \epsilon \sqrt{\tau} e^{\frac{\lambda L_0}{\epsilon\sqrt{\tau}}}$.

180 **Lemma 2.4.** (i) $\int_0^{+\infty} \left| e^{-\frac{x+\xi}{\epsilon\sqrt{\tau}}} + \operatorname{sgn}(x - \xi) e^{-\frac{|x-\xi|}{\epsilon\sqrt{\tau}}} \right| e^{\frac{\lambda x - \lambda \xi}{\epsilon\sqrt{\tau}}} d\xi \leq \frac{2\epsilon\sqrt{\tau}}{1-\lambda^2}$.

181 (ii) $\int_0^{+\infty} \left| e^{-\frac{x+\xi}{\epsilon\sqrt{\tau}}} + \operatorname{sgn}(x - \xi) e^{-\frac{|x-\xi|}{\epsilon\sqrt{\tau}}} \right| e^{\frac{\lambda x - \xi}{\epsilon\sqrt{\tau}}} d\xi \leq \epsilon\sqrt{\tau} + \frac{\epsilon\sqrt{\tau}}{e(1-\lambda)}$.

182 (iii) $\int_0^{+\infty} \left| e^{-\frac{x+\xi}{\epsilon\sqrt{\tau}}} + \operatorname{sgn}(x - \xi) e^{-\frac{|x-\xi|}{\epsilon\sqrt{\tau}}} \right| e^{\frac{\lambda x}{\epsilon\sqrt{\tau}}} |u_0(\xi)| d\xi \leq 2C_u \epsilon \sqrt{\tau} e^{\frac{\lambda L_0}{\epsilon\sqrt{\tau}}}$.

183 **Lemma 2.5.** (i) $\left| \phi_1(x) - e^{-\frac{x}{\epsilon\sqrt{\tau}}} \right| = e^{-\frac{L}{\epsilon\sqrt{\tau}}} |\phi_2(x)|$.

184 (ii) $|\phi_2(x)| \leq 1$ for $x \in [0, L]$.

185 (iii) $|\phi_2'(x)| \leq \frac{2}{\epsilon\sqrt{\tau}}$ if $\epsilon \ll 1$ for $x \in [0, L]$.

186 Last but not least, the norm that we will use in Theorem 2.1 and its proof is

$$(2.28) \quad \|Y(\cdot, t)\|_{H_{L, \epsilon, \tau}^1} := \sqrt{\int_0^L Y(x, t)^2 + (\epsilon\sqrt{\tau} Y_x(x, t))^2 dx}.$$

187 **2.3.2. A proposition.** In this section, we will give a critical estimate, which is es-
188 sential in the calculation of maximum difference $\|u_L(\cdot, t) - v_L(\cdot, t)\|_\infty$ in section
189 2.3.3. By comparing $u_L(x, t)$ and $v_L(x, t)$ given in (2.19) and (2.22) respectively,
190 it is clear that the coefficient $u(L, t) - c_1(t) e^{-\frac{L}{\epsilon\sqrt{\tau}}} - e^{-\frac{t}{\epsilon\tau}} u_0(L)$ for $\phi_2(x)$ appeared

191 in (2.19) needs to be compared with the corresponding coefficient $c_2(t)$ for $\phi_2(x)$
 192 appeared in (2.22). We thus define a space-dependent function

$$(2.29) \quad U_{c_2}(x, t) = u(x, t) - c_1(t)e^{-\frac{x}{\epsilon\sqrt{\tau}}} - e^{-\frac{t}{\epsilon\tau}}u_0(x)$$

193 and establish the following proposition

Proposition 2.6.

$$(2.30) \quad |U_{c_2}(L, t)| \leq a_\tau(t)e^{\frac{b_\tau t}{\epsilon\tau}}e^{-\frac{\lambda L}{\epsilon\sqrt{\tau}}} + c_\tau \frac{t}{\epsilon\tau}e^{\frac{(b_\tau-1)t}{\epsilon\tau}}e^{-\frac{\lambda(L-L_0)}{\epsilon\sqrt{\tau}}}$$

194 for some parameter-dependent constants a_τ , b_τ and c_τ .

195 *Proof.* Based on the implicit solution formula (2.10) derived in section 2.1, Lemma
 196 2.2 and the relationship between U_{c_2} and u given in (2.29), we can get an inequality
 197 in terms of U_{c_2}

$$(2.31) \quad \begin{aligned} |U_{c_2}(x, t)| \leq & \frac{1}{2\epsilon^2\tau\sqrt{\tau}} \left[\int_0^t \int_0^{+\infty} \left| e^{-\frac{x+\xi}{\epsilon\sqrt{\tau}}} - e^{-\frac{|x-\xi|}{\epsilon\sqrt{\tau}}} \right| |U_{c_2}(\xi, s)| e^{-\frac{t-s}{\epsilon\tau}} d\xi ds \right. \\ & + \int_0^t \int_0^{+\infty} \left| e^{-\frac{x+\xi}{\epsilon\sqrt{\tau}}} - e^{-\frac{|x-\xi|}{\epsilon\sqrt{\tau}}} \right| |c_1(s)| e^{-\frac{s}{\epsilon\sqrt{\tau}}} e^{-\frac{t-s}{\epsilon\tau}} d\xi ds \\ & + \left. \int_0^t \int_0^{+\infty} \left| e^{-\frac{x+\xi}{\epsilon\sqrt{\tau}}} - e^{-\frac{|x-\xi|}{\epsilon\sqrt{\tau}}} \right| |u_0(\xi)| e^{-\frac{t}{\epsilon\tau}} d\xi ds \right] \\ & + \frac{D}{2\epsilon^2\tau} \left[\int_0^t \int_0^{+\infty} \left| e^{-\frac{x+\xi}{\epsilon\sqrt{\tau}}} + \operatorname{sgn}(x-\xi)e^{-\frac{|x-\xi|}{\epsilon\sqrt{\tau}}} \right| |U_{c_2}(\xi, s)| e^{-\frac{t-s}{\epsilon\tau}} d\xi ds \right. \\ & + \int_0^t \int_0^{+\infty} \left| e^{-\frac{x+\xi}{\epsilon\sqrt{\tau}}} + \operatorname{sgn}(x-\xi)e^{-\frac{|x-\xi|}{\epsilon\sqrt{\tau}}} \right| |c_1(s)| e^{-\frac{s}{\epsilon\sqrt{\tau}}} e^{-\frac{t-s}{\epsilon\tau}} d\xi ds \\ & + \left. \int_0^t \int_0^{+\infty} \left| e^{-\frac{x+\xi}{\epsilon\sqrt{\tau}}} + \operatorname{sgn}(x-\xi)e^{-\frac{|x-\xi|}{\epsilon\sqrt{\tau}}} \right| |u_0(\xi)| e^{-\frac{t}{\epsilon\tau}} d\xi ds \right]. \end{aligned}$$

198 To show that $U_{c_2}(x, t)$ decays exponentially with respect to x , we pull out an
 199 exponential term by writing $U_{c_2}(x, t) = e^{-\frac{\lambda x}{\epsilon\sqrt{\tau}}}e^{-\frac{t}{\epsilon\tau}}\tilde{U}(x, t)$, where $0 < \lambda < 1$, such
 200 that

$$(2.32) \quad \tilde{U}(x, t) = e^{\frac{\lambda x}{\epsilon\sqrt{\tau}}}e^{\frac{t}{\epsilon\tau}}U_{c_2}(x, t),$$

201 then (2.31) can be rewritten in terms of $\tilde{U}(x, t)$ as follows

$$(2.33) \quad \begin{aligned} |\tilde{U}(x, t)| \leq & \frac{1}{2\epsilon^2\tau\sqrt{\tau}} \left[\int_0^t \int_0^{+\infty} \left| e^{-\frac{x+\xi}{\epsilon\sqrt{\tau}}} - e^{-\frac{|x-\xi|}{\epsilon\sqrt{\tau}}} \right| e^{\frac{\lambda x - \lambda\xi}{\epsilon\sqrt{\tau}}} |\tilde{U}(\xi, s)| d\xi ds \right. \\ & + \int_0^t \int_0^{+\infty} \left| e^{-\frac{x+\xi}{\epsilon\sqrt{\tau}}} - e^{-\frac{|x-\xi|}{\epsilon\sqrt{\tau}}} \right| |c_1(s)| e^{\frac{\lambda x - \xi}{\epsilon\sqrt{\tau}}} e^{\frac{s}{\epsilon\tau}} d\xi ds \\ & + \left. \int_0^t \int_0^{+\infty} \left| e^{-\frac{x+\xi}{\epsilon\sqrt{\tau}}} - e^{-\frac{|x-\xi|}{\epsilon\sqrt{\tau}}} \right| e^{\frac{\lambda x}{\epsilon\sqrt{\tau}}} |u_0(\xi)| d\xi ds \right] \\ & + \frac{D}{2\epsilon^2\tau} \left[\int_0^t \int_0^{+\infty} \left| e^{-\frac{x+\xi}{\epsilon\sqrt{\tau}}} + \operatorname{sgn}(x-\xi)e^{-\frac{|x-\xi|}{\epsilon\sqrt{\tau}}} \right| e^{\frac{\lambda x - \lambda\xi}{\epsilon\sqrt{\tau}}} |\tilde{U}(\xi, s)| d\xi ds \right. \\ & + \int_0^t \int_0^{+\infty} \left| e^{-\frac{x+\xi}{\epsilon\sqrt{\tau}}} + \operatorname{sgn}(x-\xi)e^{-\frac{|x-\xi|}{\epsilon\sqrt{\tau}}} \right| |c_1(s)| e^{\frac{\lambda x - \xi}{\epsilon\sqrt{\tau}}} e^{\frac{s}{\epsilon\tau}} d\xi ds \\ & + \left. \int_0^t \int_0^{+\infty} \left| e^{-\frac{x+\xi}{\epsilon\sqrt{\tau}}} + \operatorname{sgn}(x-\xi)e^{-\frac{|x-\xi|}{\epsilon\sqrt{\tau}}} \right| e^{\frac{\lambda x}{\epsilon\sqrt{\tau}}} |u_0(\xi)| d\xi ds \right]. \end{aligned}$$

202 Because of Lemmas 2.3–2.4, we can get the following estimate for $\left|\tilde{U}(\cdot, t)\right|_{\infty}$ based
 203 on (2.33) :

$$\begin{aligned}
 \left|\tilde{U}(\cdot, t)\right|_{\infty} &\leq \frac{1}{2\epsilon^2\tau\sqrt{\tau}} \left[\frac{2\epsilon\sqrt{\tau}}{1-\lambda^2} \int_0^t |\tilde{U}(\cdot, s)|_{\infty} ds + \frac{\epsilon\sqrt{\tau}}{e(1-\lambda)} \int_0^t |c_1(s)|e^{\frac{s}{\epsilon\tau}} ds \right. \\
 &\quad \left. + 2C_u\epsilon\sqrt{\tau}e^{\frac{\lambda L_0}{\epsilon\sqrt{\tau}}} \int_0^t 1 ds \right] \\
 (2.34) \quad &+ \frac{D}{2\epsilon^2\tau} \left[\frac{2\epsilon\sqrt{\tau}}{1-\lambda^2} \int_0^t |\tilde{U}(\cdot, s)|_{\infty} ds + \epsilon\sqrt{\tau} \left(1 + \frac{1}{e(1-\lambda)}\right) \int_0^t |c_1(s)|e^{\frac{s}{\epsilon\tau}} ds \right. \\
 &\quad \left. + 2C_u\epsilon\sqrt{\tau}e^{\frac{\lambda L_0}{\epsilon\sqrt{\tau}}} \int_0^t 1 ds \right] \\
 &\leq \int_0^t \frac{b_{\tau}}{\epsilon\tau} |\tilde{U}(\cdot, s)|_{\infty} ds + \int_0^t \frac{\tilde{a}_{\tau}(s)}{\epsilon\tau} ds
 \end{aligned}$$

where

$$\begin{aligned}
 b_{\tau} &= \frac{1 + D\sqrt{\tau}}{1 - \lambda^2}, & \tilde{a}_{\tau}(t) &= a_{\tau}e^{\frac{t}{\epsilon\tau}} + c_{\tau}e^{\frac{\lambda L_0}{\epsilon\sqrt{\tau}}}, \\
 a_{\tau} &= \frac{|c_1(\cdot)|_{\infty}(1 + D\sqrt{\tau}(e(1-\lambda) + 1))}{2e(1-\lambda)}, & c_{\tau} &= C_u(1 + D\sqrt{\tau}).
 \end{aligned}$$

By Gronwall's inequality, inequality (2.34) gives that

$$\left|\tilde{U}(\cdot, t)\right|_{\infty} \leq \int_0^t \frac{\tilde{a}_{\tau}(t-s)}{\epsilon\tau} e^{\frac{b_{\tau}(t-s)}{\epsilon\tau}} ds \leq \left(a_{\tau}e^{\frac{t}{\epsilon\tau}} + c_{\tau}\frac{t}{\epsilon\tau}e^{\frac{\lambda L_0}{\epsilon\sqrt{\tau}}}\right) e^{\frac{b_{\tau}t}{\epsilon\tau}}$$

204 Hence $|U_{c_2}(x, t)| \leq \left|\tilde{U}(\cdot, t)\right|_{\infty} e^{\frac{-\lambda x}{\epsilon\sqrt{\tau}}} e^{-\frac{t}{\epsilon\tau}} \leq \left(a_{\tau}e^{\frac{t}{\epsilon\tau}} + c_{\tau}\frac{t}{\epsilon\tau}e^{\frac{\lambda L_0}{\epsilon\sqrt{\tau}}}\right) e^{\frac{b_{\tau}t}{\epsilon\tau}} e^{\frac{-\lambda x}{\epsilon\sqrt{\tau}}} e^{-\frac{t}{\epsilon\tau}}$ i.e.,
 205 $U_{c_2}(x, t)$ decays exponentially with respect to x . In particular, when $x = L$, we
 206 have

$$(2.35) \quad |U_{c_2}(L, t)| \leq a_{\tau}e^{\frac{b_{\tau}t}{\epsilon\tau}} e^{-\frac{\lambda L}{\epsilon\sqrt{\tau}}} + c_{\tau}\frac{t}{\epsilon\tau} e^{\frac{(b_{\tau}-1)t}{\epsilon\tau}} e^{-\frac{\lambda(L-L_0)}{\epsilon\sqrt{\tau}}}$$

207 as given in (2.30). □

208 **2.3.3. Proof of Theorem 2.1.** In this section, we will first find the maximum dif-
 209 ference of $\|u_L(\cdot, t) - v_L(\cdot, t)\|_{\infty}$, then we will derive $\|u_L(\cdot, t) - v_L(\cdot, t)\|_{H_{L,\epsilon,\tau}^1}$ and
 210 $\|W(\cdot, t)\|_{H_{L,\epsilon,\tau}^1} = \|U(\cdot, t) - V(\cdot, t)\|_{H_{L,\epsilon,\tau}^1}$. Combining these two, we will get an
 211 estimate for $\|u(\cdot, t) - v(\cdot, t)\|_{H_{L,\epsilon,\tau}^1}$.

Proposition 2.7. *If $u_0(x)$ satisfies (2.27), then*

$$\|u_L - v_L\|_{\infty} \leq E_{1;\epsilon,\tau}(t)e^{-\frac{\lambda L}{\epsilon\sqrt{\tau}}} + E_{2;\epsilon,\tau}(t)e^{-\frac{\lambda(L-L_0)}{\epsilon\sqrt{\tau}}}$$

212 where $E_{1;\epsilon,\tau}(t) = |c_1(\cdot)|_{\infty} + a_{\tau}e^{\frac{b_{\tau}t}{\epsilon\tau}}$ and $E_{2;\epsilon,\tau}(t) = c_{\tau}\frac{t}{\epsilon\tau}e^{\frac{(b_{\tau}-1)t}{\epsilon\tau}}$.

Proof. By the definition of u_L and v_L given in (2.19) and (2.22) and the assumption that $u_0(x) = v_0(x)$ for $x \in [0, L]$, we can get their difference

$$u_L(x, t) - v_L(x, t) = c_1(t) \left(e^{-\frac{x}{\epsilon\sqrt{\tau}}} - \phi_1(x) \right) + \left(U_{c_2}(L, t) - h(t) + e^{-\frac{t}{\epsilon\tau}} h(0) \right) \phi_2(x)$$

213 Combining Lemmas 2.5(i), 2.5(ii), inequality (2.35), and $h(t) \equiv 0$, we have

$$(2.36) \quad \|u_L(\cdot, t) - v_L(\cdot, t)\|_{\infty} \leq E_{1;\epsilon,\tau}(t)e^{-\frac{\lambda L}{\epsilon\sqrt{\tau}}} + E_{2;\epsilon,\tau}(t)e^{-\frac{\lambda(L-L_0)}{\epsilon\sqrt{\tau}}}$$

214 where

$$(2.37) \quad E_{1;\epsilon,\tau}(t) = |c_1(\cdot)|_\infty + a_\tau e^{\frac{b_\tau t}{\epsilon\tau}} \quad \text{and} \quad E_{2;\epsilon,\tau}(t) = c_\tau \frac{t}{\epsilon\tau} e^{\frac{(b_\tau-1)t}{\epsilon\tau}}.$$

215

□

Proposition 2.8. *If $u_0(x)$ satisfies (2.27), and $E_{1;\epsilon,\tau}(t), E_{2;\epsilon,\tau}(t)$ are as in proposition 2.7, then*

$$\|u_L(\cdot, t) - v_L(\cdot, t)\|_{H_{L,\epsilon,\tau}^1} \leq \sqrt{5L} \left(E_{1;\epsilon,\tau}(t) e^{-\frac{\lambda L}{\epsilon\sqrt{\tau}}} + E_{2;\epsilon,\tau}(t) e^{-\frac{\lambda(L-L_0)}{\epsilon\sqrt{\tau}}} \right).$$

216

217 *Proof.* Because of the definition of u_L and v_L given in (2.19) and (2.22), Lemma
218 2.5(iii) and inequality (2.35), we have that

$$(2.38) \quad \begin{aligned} \|u_L(\cdot, t) - v_L(\cdot, t)\|_x &\leq |c_1(t)| e^{-\frac{L}{\epsilon\sqrt{\tau}}} |\phi_2'(x)| + |U_{c_2}(L, t)| |\phi_2'(x)| \\ &\leq \frac{2}{\epsilon\sqrt{\tau}} \left(E_{1;\epsilon,\tau}(t) e^{-\frac{\lambda L}{\epsilon\sqrt{\tau}}} + E_{2;\epsilon,\tau}(t) e^{-\frac{\lambda(L-L_0)}{\epsilon\sqrt{\tau}}} \right). \end{aligned}$$

219 Now, combining (2.36) and (2.38), we obtain that

$$(2.39) \quad \begin{aligned} \|u_L(\cdot, t) - v_L(\cdot, t)\|_{H_{L,\epsilon,\tau}^1} &= \sqrt{\int_0^L |u_L - v_L|^2 + |\epsilon\sqrt{\tau}(u_L - v_L)_x|^2 dx} \\ &\leq \sqrt{5L} \left(E_{1;\epsilon,\tau}(t) e^{-\frac{\lambda L}{\epsilon\sqrt{\tau}}} + E_{2;\epsilon,\tau}(t) e^{-\frac{\lambda(L-L_0)}{\epsilon\sqrt{\tau}}} \right). \end{aligned}$$

220

□

Proposition 2.9. *If $u_0(x)$ satisfies (2.27), then*

$$\|W(\cdot, t)\|_{H_{L,\epsilon,\tau}^1} \leq \gamma_{1;\epsilon,\tau}(t) e^{-\frac{\lambda L}{\epsilon\sqrt{\tau}}} + \gamma_{2;\epsilon,\tau}(t) e^{-\frac{\lambda(L-L_0)}{\epsilon\sqrt{\tau}}}$$

221 where the coefficients are given by

$$(2.40) \quad \begin{aligned} \gamma_{1;\epsilon,\tau}(t) &= e^{\frac{(M+1)^2 t}{2M\epsilon\sqrt{\tau}}} \left(\frac{(M+1)^2 \sqrt{\tau}}{2M} + 1 \right) \sqrt{L} \left(\frac{t}{\epsilon\tau} |c_1(\cdot)|_\infty + \frac{a_\tau}{b_\tau} \left(e^{\frac{b_\tau t}{\epsilon\tau}} - 1 \right) \right) \\ \gamma_{2;\epsilon,\tau}(t) &= e^{\frac{(M+1)^2 t}{2M\epsilon\sqrt{\tau}}} \left(\frac{(M+1)^2 \sqrt{\tau}}{2M} + 1 \right) \sqrt{L} c_\tau \\ &\quad \cdot \left(\frac{t}{\epsilon\tau(b_\tau-1)} e^{\frac{(b_\tau-1)t}{\epsilon\tau}} - \frac{1}{(b_\tau-1)^2} \left(e^{\frac{(b_\tau-1)t}{\epsilon\tau}} - 1 \right) \right). \end{aligned}$$

222

223 *Proof.* Multiplying the governing equation of W (2.25) by $2W$, integrating over
224 $[0, L]$, and using integration by parts, we get

$$\begin{aligned} &\frac{d}{dt} \int_0^L W^2 + (\epsilon\sqrt{\tau} W_x)^2 dx \\ &= -\epsilon \int_0^L 2W_x^2 dx + \int_0^L 2W_x (f(v) - f(u)) dx + \frac{2}{\epsilon\tau} \int_0^L W(v_L - u_L) dx. \end{aligned}$$

225 Therefore, using the norm we defined earlier in (2.28), and $f'(u) \leq \frac{(M+1)^2}{2M} := C$,
 226 we have

$$\begin{aligned}
 & \frac{d}{dt} \|W(\cdot, t)\|_{H_{L,\epsilon,\tau}^1}^2 \\
 & \leq 2 \int_0^L |W_x| |f'(\eta)| |v - u| dx + \frac{2\sqrt{L}}{\epsilon\tau} \|v_L - u_L\|_\infty \|W(\cdot, t)\|_{H_{L,\epsilon,\tau}^1} \\
 & \leq 2C \int_0^L |W_x| (|W| + \|v_L - u_L\|_\infty) dx + \frac{2\sqrt{L}}{\epsilon\tau} \|v_L - u_L\|_\infty \|W(\cdot, t)\|_{H_{L,\epsilon,\tau}^1} \\
 & \leq \frac{2C}{\epsilon\sqrt{\tau}} \left(\|W(\cdot, t)\|_{H_{L,\epsilon,\tau}^1}^2 + \|v_L - u_L\|_\infty \sqrt{L} \|W(\cdot, t)\|_{H_{L,\epsilon,\tau}^1} \right) \\
 & \quad + \frac{2\sqrt{L}}{\epsilon\tau} \|v_L - u_L\|_\infty \|W(\cdot, t)\|_{H_{L,\epsilon,\tau}^1} \\
 & = \frac{2C}{\epsilon\sqrt{\tau}} \|W(\cdot, t)\|_{H_{L,\epsilon,\tau}^1}^2 + \left(\frac{2C}{\epsilon\sqrt{\tau}} + \frac{2}{\epsilon\tau} \right) \sqrt{L} \|v_L - u_L\|_\infty \|W(\cdot, t)\|_{H_{L,\epsilon,\tau}^1}.
 \end{aligned}$$

Hence,

$$\frac{d}{dt} \|W(\cdot, t)\|_{H_{L,\epsilon,\tau}^1} \leq \frac{C}{\epsilon\sqrt{\tau}} \|W(\cdot, t)\|_{H_{L,\epsilon,\tau}^1} + \left(\frac{C}{\epsilon\sqrt{\tau}} + \frac{1}{\epsilon\tau} \right) \sqrt{L} \|v_L - u_L\|_\infty.$$

227 By Gronwall's inequality and (2.36)

$$\begin{aligned}
 & \|W(\cdot, t)\|_{H_{L,\epsilon,\tau}^1} \\
 & \leq \int_0^t \left(\frac{C}{\epsilon\sqrt{\tau}} + \frac{1}{\epsilon\tau} \right) \sqrt{L} \|v_L - u_L\|_\infty e^{\frac{C(t-s)}{\epsilon\sqrt{\tau}}} ds \\
 & \leq e^{\frac{Ct}{\epsilon\sqrt{\tau}}} \left(\frac{C}{\epsilon\sqrt{\tau}} + \frac{1}{\epsilon\tau} \right) \sqrt{L} \int_0^t E_{1;\epsilon,\tau}(s) e^{-\frac{\lambda L}{\epsilon\sqrt{\tau}}} + E_{2;\epsilon,\tau}(s) e^{-\frac{\lambda(L-L_0)}{\epsilon\sqrt{\tau}}} ds \\
 & \leq \left(e^{\frac{Ct}{\epsilon\sqrt{\tau}}} \left(\frac{C}{\epsilon\sqrt{\tau}} + \frac{1}{\epsilon\tau} \right) \sqrt{L} \int_0^t E_{1;\epsilon,\tau}(s) ds \right) e^{-\frac{\lambda L}{\epsilon\sqrt{\tau}}} \\
 & \quad + \left(e^{\frac{Ct}{\epsilon\sqrt{\tau}}} \left(\frac{C}{\epsilon\sqrt{\tau}} + \frac{1}{\epsilon\tau} \right) \sqrt{L} \int_0^t E_{2;\epsilon,\tau}(s) ds \right) e^{-\frac{\lambda(L-L_0)}{\epsilon\sqrt{\tau}}} \\
 & \leq e^{\frac{Ct}{\epsilon\sqrt{\tau}}} \left(\frac{C}{\epsilon\sqrt{\tau}} + \frac{1}{\epsilon\tau} \right) \sqrt{L} \left(t |c_1(\cdot)|_\infty + \frac{a_\tau \epsilon \tau}{b_\tau} (e^{\frac{b_\tau t}{\epsilon\tau}} - 1) \right) e^{-\frac{\lambda L}{\epsilon\sqrt{\tau}}} \\
 & \quad + e^{\frac{Ct}{\epsilon\sqrt{\tau}}} \left(\frac{C}{\epsilon\sqrt{\tau}} + \frac{1}{\epsilon\tau} \right) \sqrt{L} \frac{c_\tau}{\epsilon\tau} \left(\frac{\epsilon\tau}{b_\tau - 1} t e^{\frac{(b_\tau - 1)t}{\epsilon\tau}} - \left(\frac{\epsilon\tau}{b_\tau - 1} \right)^2 (e^{\frac{(b_\tau - 1)t}{\epsilon\tau}} - 1) \right) e^{-\frac{\lambda(L-L_0)}{\epsilon\sqrt{\tau}}}.
 \end{aligned}$$

Hence

$$\|W(\cdot, t)\|_{H_{L,\epsilon,\tau}^1} \leq \gamma_{1;\epsilon,\tau}(t) e^{-\frac{\lambda L}{\epsilon\sqrt{\tau}}} + \gamma_{2;\epsilon,\tau}(t) e^{-\frac{\lambda(L-L_0)}{\epsilon\sqrt{\tau}}}$$

228 where $\gamma_{1;\epsilon,\tau}(t)$ and $\gamma_{2;\epsilon,\tau}(t)$ are given in (2.40). □

229 Now we are in the position to prove the main theorem of this section.

230 **Theorem 2.10.** *If $u_0(x)$ satisfies*

$$u_0(x) = \begin{cases} C_u & x \in [0, L_0] \\ 0 & x > L_0 \end{cases}$$

231 where $L_0 < L$ and C_u , are positive constants, and $E_{1;\epsilon,\tau}(t), E_{2;\epsilon,\tau}(t), \gamma_{1;\epsilon,\tau}(t), \gamma_{2;\epsilon,\tau}(t)$
 232 are as in (2.37) and (2.40), then

$$(2.41) \quad \|u(\cdot, t) - v(\cdot, t)\|_{H_{L,\epsilon,\tau}^1} \leq D_{1;\epsilon,\tau}(t)e^{-\frac{\lambda L}{\epsilon\sqrt{\tau}}} + D_{2;\epsilon,\tau}(t)e^{-\frac{\lambda(L-L_0)}{\epsilon\sqrt{\tau}}}$$

for some $0 < \lambda < 1$, and

$$D_{1;\epsilon,\tau}(t) = \gamma_{1;\epsilon,\tau}(t) + \sqrt{5L}E_{1;\epsilon,\tau}(t), \quad D_{2;\epsilon,\tau}(t) = \gamma_{2;\epsilon,\tau}(t) + \sqrt{5L}E_{2;\epsilon,\tau}(t).$$

Proof of the Main Theorem.

$$\begin{aligned} \|u(\cdot, t) - v(\cdot, t)\|_{H_{L,\epsilon,\tau}^1} &\leq \|W(\cdot, t)\|_{H_{L,\epsilon,\tau}^1} + \|v_L(\cdot, t) - u_L(\cdot, t)\|_{H_{L,\epsilon,\tau}^1} \\ &= D_{1;\epsilon,\tau}(t)e^{-\frac{\lambda L}{\epsilon\sqrt{\tau}}} + D_{2;\epsilon,\tau}(t)e^{-\frac{\lambda(L-L_0)}{\epsilon\sqrt{\tau}}} \end{aligned}$$

where

$$\begin{aligned} D_{1;\epsilon,\tau}(t) &= \gamma_{1;\epsilon,\tau}(t) + \sqrt{5L}E_{1;\epsilon,\tau}(t) \\ &= e^{\frac{(M+1)^2 t}{2M\epsilon\sqrt{\tau}}} \left(\frac{(M+1)^2 \sqrt{\tau}}{2M} + 1 \right) \sqrt{L} \left(\frac{t}{\epsilon\tau} |c_1(\cdot)|_\infty + \frac{a_\tau}{b_\tau} (e^{\frac{b_\tau t}{\epsilon\tau}} - 1) \right) \\ &\quad + \sqrt{5L}(|c(\cdot)|_\infty + a_\tau e^{\frac{b_\tau t}{\epsilon\tau}}), \\ D_{2;\epsilon,\tau}(t) &= \gamma_{2;\epsilon,\tau}(t) + \sqrt{5L}E_{2;\epsilon,\tau}(t) \\ &= e^{\frac{(M+1)^2 t}{2M\epsilon\sqrt{\tau}}} \left(\frac{(M+1)^2 \sqrt{\tau}}{2M} + 1 \right) \sqrt{L}c_\tau \cdot \\ &\quad \cdot \left(\frac{t}{\epsilon\tau(b_\tau - 1)} e^{\frac{(b_\tau - 1)t}{\epsilon\tau}} - \frac{1}{(b_\tau - 1)^2} (e^{\frac{(b_\tau - 1)t}{\epsilon\tau}} - 1) \right) \\ &\quad + \sqrt{5L}c_\tau \frac{t}{\epsilon\tau} e^{\frac{(b_\tau - 1)t}{\epsilon\tau}}. \end{aligned}$$

233

□

234 This result gives that $\|u(\cdot, t) - v(\cdot, t)\|_{H_{L,\epsilon,\tau}^1}$ exponentially delays in L . This
 235 theorem shows that if $\frac{\lambda L}{\epsilon\sqrt{\tau}}$ and $\frac{\lambda(L-L_0)}{\epsilon\sqrt{\tau}}$ converge to infinity, then the solution
 236 $v(x, t)$ of the finite interval problem converges to the solution $u(x, t)$ of the half
 237 line problem in the sense of $\|\cdot\|_{H_{L,\epsilon,\tau}^1}$. This can be achieved either by letting
 238 $L \rightarrow \infty$ or $\epsilon \rightarrow 0$. For example, in the extreme case, $\epsilon = 0$, the half line problem
 239 (1.11) becomes hyperbolic and the domain of dependence is finite, so, certainly, one
 240 only need to consider the finite interval problem. This is consistent with the main
 241 theorem in the sense that for a fixed final time t , if $\lambda L > b_\tau t$ and $\lambda(L - L_0) >$
 242 $(b_\tau - 1)t$, i.e., $L > \max(\frac{b_\tau t}{\lambda}, \frac{(b_\tau - 1)t}{\lambda})$, then $\|u(\cdot, t) - v(\cdot, t)\|_{H_{L,\epsilon,\tau}^1} \leq D_{1;\epsilon,\tau}(t)e^{-\frac{\lambda L}{\epsilon\sqrt{\tau}}} +$
 243 $D_{2;\epsilon,\tau}(t)e^{-\frac{\lambda(L-L_0)}{\epsilon\sqrt{\tau}}} \rightarrow 0$ as $\epsilon \rightarrow 0$. Theorem 2.10 gives a theoretical justification for
 244 using the solution of the finite interval problem to approximate the solution of the
 245 half line problem with appropriate choice of L and ϵ . Hence in the next chapter,
 246 the numerical scheme designed to solve the MBL equation (1.10) is given for finite
 247 interval problem.

248

3. NUMERICAL SCHEMES

249 To numerically solve the MBL equation (1.10), We first collect all the terms with
250 time derivative and rewrite MBL equation (1.10) as

$$(3.1) \quad (u - \epsilon^2 \tau u_{xx})_t + (f(u))_x = \epsilon u_{xx}.$$

251 By letting

$$(3.2) \quad w = u - \epsilon^2 \tau u_{xx} \iff u = (I - \epsilon^2 \tau \partial_{xx})^{-1} w,$$

252 MBL equation (3.1) can be written as

$$(3.3) \quad w_t + (f(u))_x = \epsilon u_{xx}.$$

253 Now, the new form of MBL equation (3.3) can be viewed as a PDE in terms of w ,
254 and the occurrence of u can be recovered by (3.2). Equation (3.3) can be formally
255 viewed as

$$(3.4) \quad w_t + (f((I - \epsilon^2 \tau \partial_{xx})^{-1} w))_x = \epsilon ((I - \epsilon^2 \tau \partial_{xx})^{-1} w)_{xx},$$

256 which is a balance law in term of w . We adopt numerical schemes originally designed
257 for hyperbolic equations to solve the MBL equation (3.1), which is of pseudo-
258 parabolic type. The local discontinuous Galerkin method has been applied to solve
259 equations involving mixed derivatives u_{xxt} term [23, 24]. To the best knowledge of
260 the authors, the central schemes have not been applied to solve equations of this
261 kind. The main advantage of the central schemes is the simplicity. “the direction of
262 the wind“ is not required to be identified, and hence the field-by-field decomposition
263 can be avoided. In this chapter, we demonstrate how to apply the central schemes
264 to solve the MBL equation (3.1).

265 **3.1. Second-order schemes.** In this section, we show how to apply the classical
266 second order central schemes [18] originally designed for hyperbolic conservation
267 laws to numerically solve the MBL equation (1.10), which is of pseudo-parabolic
268 type. To solve (3.3), we modify the central scheme given in [18]. As in [18], at each
269 time level, we first reconstruct a piecewise linear approximation of the form

$$(3.5) \quad L_j(x, t) = w_j(t) + (x - x_j) \frac{w'_j}{\Delta x}, \quad x_{j-\frac{1}{2}} \leq x \leq x_{j+\frac{1}{2}}.$$

270 Second-order accuracy is guaranteed if the so-called vector of numerical derivative
271 $\frac{w'_j}{\Delta x}$, which will be given later, satisfies

$$(3.6) \quad \frac{w'_j}{\Delta x} = \frac{\partial w(x_j, t)}{\partial x} + O(\Delta x).$$

272 We denote the staggered piecewise-constant functions $\bar{w}_{j+\frac{1}{2}}(t)$ as

$$(3.7) \quad \bar{w}_{j+\frac{1}{2}}(t) = \frac{1}{\Delta x} \int_{x_j}^{x_{j+1}} w(x, t) dx.$$

273 Evolve the piecewise linear interpolant (3.5) by integrating (3.3) over $[x_j, x_{j+1}] \times$
 274 $[t, t + \Delta t]$

$$(3.8) \quad \begin{aligned} \bar{w}_{j+\frac{1}{2}}(t + \Delta t) = & \bar{w}_{j+\frac{1}{2}}(t) \\ & - \frac{1}{\Delta x} \left[\int_t^{t+\Delta t} f(u(x_{j+1}, s)) ds - \int_t^{t+\Delta t} f(u(x_j, s)) ds \right] \\ & + \frac{\epsilon}{\Delta x} \left[\int_t^{t+\Delta t} \int_{x_j}^{x_{j+1}} \frac{\partial^2 u(x, s)}{\partial x^2} dx ds \right]. \end{aligned}$$

275 We calculate each term on the right hand side of (3.8) below. For $\bar{w}_{j+\frac{1}{2}}(t)$, applying
 276 the definition of $L_j(x, t)$ and $L_{j+1}(x, t)$ given in (3.5) to (3.7), we have that

$$(3.9) \quad \begin{aligned} \bar{w}_{j+\frac{1}{2}}(t) &= \frac{1}{\Delta x} \int_{x_j}^{x_{j+\frac{1}{2}}} L_j(x, t) dx + \frac{1}{\Delta x} \int_{x_{j+\frac{1}{2}}}^{x_{j+1}} L_{j+1}(x, t) dx \\ &= \frac{1}{2}(w_j(t) + w_{j+1}(t)) + \frac{1}{8}(w'_j - w'_{j+1}). \end{aligned}$$

277 The middle two integrands can be approximated by the midpoint rule

$$(3.10) \quad \begin{aligned} \int_t^{t+\Delta t} f(u(x_j, s)) ds &= f(u(x_j, t + \frac{\Delta t}{2}))\Delta t + O(\Delta t^3) \\ \int_t^{t+\Delta t} f(u(x_{j+1}, s)) ds &= f(u(x_{j+1}, t + \frac{\Delta t}{2}))\Delta t + O(\Delta t^3) \end{aligned}$$

if the CFL condition

$$\lambda \cdot \max_{x_j \leq x \leq x_{j+1}} \left| \frac{\partial f(u(w(x, t)))}{\partial w} \right| < \frac{1}{2}, \quad \text{where } \lambda = \frac{\Delta t}{\Delta x}$$

is met. For MBL equation (3.3), we have that at $t > 0$,

$$u - \epsilon^2 \tau u_{xx} = w, \quad u(0) = w(0), \quad u(L) = w(L).$$

Let $v(x) = \frac{(L-x)w(0) + xw(L)}{L}$, then

$$u(x) = [Iw](x) = v(x) + \frac{1}{L} \int_0^L [w(y) - v(y)] K(x, y) dy$$

where

$$K(x, y) = \sum_{k=1}^{\infty} \frac{\sin(\frac{k\pi x}{L}) \sin(\frac{k\pi y}{L})}{1 + (\frac{k\pi}{L})^2 \epsilon^2 \tau}.$$

Hence the eigenvalues for I are

$$\lambda_k = \frac{1}{1 + (\frac{k\pi}{L})^2 \epsilon^2 \tau} \leq 1, \quad k = 1, 2, 3, \dots$$

Therefore, the CFL condition is

$$\frac{\Delta t}{\Delta x} \cdot \max_{x_j \leq x \leq x_{j+1}} \left| \frac{\partial f(u(w(x, t)))}{\partial w} \right| = \frac{\Delta t}{\Delta x} \cdot \max_{k=1,2,3,\dots} \left| \frac{\partial f(u(x, t))}{\partial u} \right| \cdot \lambda_k \leq \frac{\Delta t}{\Delta x} \cdot 2.2 < \frac{1}{2}$$

278 In the numerical computations in chapter 4, we chose $\frac{\Delta t}{\Delta x} = 0.1$. In (3.10), to
 279 estimate $u(\cdot, t + \frac{\Delta t}{2})$'s, we use Taylor expansion and the conservation law (3.3):

$$\begin{aligned}
 (3.11) \quad w(x_j, t + \frac{\Delta t}{2}) &= w_j(t) + \frac{\partial w}{\partial t} \frac{\Delta t}{2} + \mathcal{O}(\Delta t^2) \\
 &= w_j(t) + (\epsilon \frac{\partial^2 u}{\partial x^2} - \frac{\partial f}{\partial x}) \frac{\Delta t}{2} + \mathcal{O}(\Delta t^2) \\
 &= w_j(t) + (\epsilon \Delta x D^2 u_j - f'_j) \frac{\lambda}{2},
 \end{aligned}$$

where D is the discrete central difference operator

$$D^2 u_j = \frac{u_{j-1} - 2u_j + u_{j+1}}{\Delta x^2},$$

280 and the second-order accuracy is met if

$$(3.12) \quad \frac{f'_j}{\Delta x} = \frac{\partial f(u(x_j, t))}{\partial x} + \mathcal{O}(\Delta x).$$

281 The choices for $\{w'_j\}$ in (3.6) and $\{f'_j\}$ in (3.12) can be found in [18], and we chose

$$(3.13) \quad w'_j = MM\{\Delta w_{j+\frac{1}{2}}, \Delta w_{j-\frac{1}{2}}\}, \quad f'_j = MM\{\Delta f_{j+\frac{1}{2}}, \Delta f_{j-\frac{1}{2}}\}$$

282 where $MM\{x, y\} = \min\text{mod}(x, y) = \frac{1}{2}(\text{sgn}(x) + \text{sgn}(y)) \cdot \text{Min}(|x|, |y|)$ and $\Delta w_{j+\frac{1}{2}} =$
 283 $w_{j+1} - w_j$. Combining (3.8)-(3.10), we obtain

$$\begin{aligned}
 (3.14) \quad \bar{w}_{j+\frac{1}{2}}(t + \Delta t) &= \bar{w}_{j+\frac{1}{2}}(t) \\
 &\quad - \lambda [f(u_{j+1}(t + \frac{\Delta t}{2})) - f(u_j(t + \frac{\Delta t}{2}))] \\
 &\quad + \frac{\epsilon}{\Delta x} \left[\int_t^{t+\Delta t} \int_{x_j}^{x_{j+1}} \frac{\partial^2 u(x, s)}{\partial x^2} dx ds \right].
 \end{aligned}$$

Next, we will re-write (3.14) in terms of u . $(\overline{u_{xx}})_{j+\frac{1}{2}}$ is approximated as

$$(\overline{u_{xx}})_{j+\frac{1}{2}} = \frac{1}{\Delta x} \int_{x_j}^{x_{j+1}} u_{xx} dx = \frac{1}{\Delta x} (u_x(x_{j+1}, t) - u_x(x_j, t)),$$

284 and using the cell averages, it becomes

$$\begin{aligned}
 (3.15) \quad (\overline{u_{xx}})_{j+\frac{1}{2}} &= \frac{1}{\Delta x} \left(\frac{\bar{u}_{j+3/2} - \bar{u}_{j+1/2}}{\Delta x} - \frac{\bar{u}_{j+1/2} - \bar{u}_{j-1/2}}{\Delta x} \right) \\
 &= \frac{\bar{u}_{j+3/2} - 2\bar{u}_{j+1/2} + \bar{u}_{j-1/2}}{(\Delta x)^2} \\
 &= D^2 \bar{u}_{j+\frac{1}{2}}.
 \end{aligned}$$

Notice that the linear interpolation (similar to (3.5))

$$\tilde{L}_{j+\frac{1}{2}}(x, t + \Delta t) = u_{j+\frac{1}{2}}(t + \Delta t) + (x - x_{j+\frac{1}{2}}) \frac{u'_{j+\frac{1}{2}}}{\Delta x} \quad \text{for } x_j \leq x \leq x_{j+1}$$

and the cell average definition (similar to (3.7))

$$\bar{u}_{j+\frac{1}{2}}(t + \Delta t) = \frac{1}{\Delta x} \int_{x_j}^{x_{j+1}} u(x, t + \Delta t) dx$$

ensure that

$$\bar{u}_{j+\frac{1}{2}}(t + \Delta t) = u_{j+\frac{1}{2}}(t + \Delta t),$$

285 and the conversion between u and w is done using the following relation

$$(3.16) \quad (I - \epsilon^2 \tau D^2)u = w.$$

286 Hence re-writting (3.14) in terms of u gives the staggered central scheme

$$(3.17) \quad \begin{aligned} (I - \epsilon^2 \tau D^2)u_{j+\frac{1}{2}}(t + \Delta t) &= (I - \epsilon^2 \tau D^2)\bar{u}_{j+\frac{1}{2}}(t) \\ &\quad - \lambda[f(u_{j+1}(t + \frac{\Delta t}{2}) - f(u_j(t + \frac{\Delta t}{2}))) \\ &\quad + \frac{\epsilon}{\Delta x} \left[\int_t^{t+\Delta t} \int_{x_j}^{x_{j+1}} \frac{\partial^2 u(x, s)}{\partial x^2} dx ds \right]]. \end{aligned}$$

287 We will focus on the last integral in (3.17). There are many ways to numerically
288 calculate this integral. We will show two ways to do this in the following two
289 subsections, both of them achieve second order accuracy.

290 3.1.1. *Trapezoid Scheme.* In this scheme, we use the notion (3.7) and the trapezoid
291 rule to calculate the integral numerically as follows:

$$(3.18) \quad \begin{aligned} \int_t^{t+\Delta t} \int_{x_j}^{x_{j+1}} \frac{\partial^2 u(x, s)}{\partial x^2} dx ds &= \Delta x \int_t^{t+\Delta t} (\bar{u}_{xx})_{j+\frac{1}{2}}(s) ds \\ &= \frac{\Delta x \Delta t}{2} \left((\bar{u}_{xx})_{j+\frac{1}{2}}(t) + (\bar{u}_{xx})_{j+\frac{1}{2}}(t + \Delta t) \right) \end{aligned}$$

292 with $\mathcal{O}(\Delta t^3)$ error. Combining with (3.15) and (3.17), we can get the trapezoid
293 scheme

$$(3.19) \quad \begin{aligned} \left(I - (\epsilon^2 \tau + \frac{\epsilon \Delta t}{2}) D^2 \right) u_{j+\frac{1}{2}}(t + \Delta t) &= \left(I - (\epsilon^2 \tau - \frac{\epsilon \Delta t}{2}) D^2 \right) \bar{u}_{j+\frac{1}{2}}(t) \\ &\quad - \lambda \left[f(u_{j+1}(t + \frac{\Delta t}{2})) - f(u_j(t + \frac{\Delta t}{2})) \right] \end{aligned}$$

294 The flow chart of the trapezoid scheme is given in (3.20)

$$(3.20) \quad \begin{array}{ccccc} & & (3.9) & \bar{w}_{j+\frac{1}{2}}(t) & \xrightarrow{(3.16)} & \bar{u}_{j+\frac{1}{2}}(t) & \xrightarrow{(3.19)} & & \\ & & & & & & & & \\ u_j(t) & \xrightarrow{(3.16)} & w_j(t) & \begin{array}{l} \nearrow \\ \searrow \end{array} & & & & & u_{j+\frac{1}{2}}(t + \Delta t) \\ & & & (3.11) & w_j(t + \frac{\Delta t}{2}) & \xrightarrow{(3.16)} & u_j(t + \frac{\Delta t}{2}) & \xrightarrow{(3.19)} & \end{array}$$

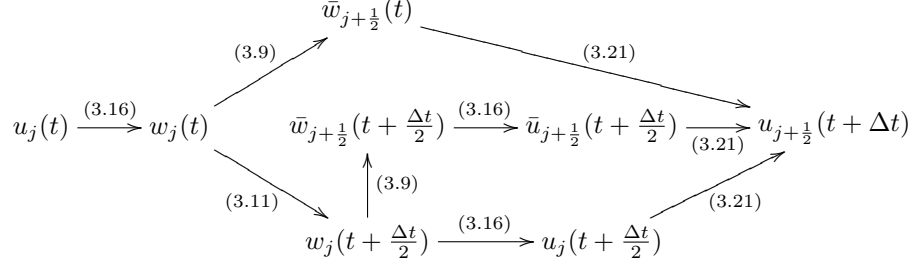
3.1.2. *Midpoint Scheme.* In this scheme, we use the notion (3.7) and the midpoint
rule to calculate the integral numerically as follows:

$$\begin{aligned} \int_t^{t+\Delta t} \int_{x_j}^{x_{j+1}} \frac{\partial^2 u(x, s)}{\partial x^2} dx ds &= \Delta x \int_t^{t+\Delta t} (\bar{u}_{xx})_{j+\frac{1}{2}}(s) ds \\ &= \Delta x \Delta t (\bar{u}_{xx})_{j+\frac{1}{2}}(t + \frac{\Delta t}{2}) \end{aligned}$$

295 Combining with (3.15) and (3.17), we can get the midpoint scheme

$$(3.21) \quad \begin{aligned} (I - \epsilon^2 \tau D^2)u_{j+\frac{1}{2}}(t + \Delta t) &= \bar{w}_{j+\frac{1}{2}}(t) \\ &\quad - \lambda[f(u_{j+1}(t + \frac{\Delta t}{2}) - f(u_j(t + \frac{\Delta t}{2}))) \\ &\quad + \epsilon \Delta t D^2 \bar{u}_{j+\frac{1}{2}}(t + \frac{\Delta t}{2})] \end{aligned}$$

296 The flow chart of the midpoint scheme is given in (3.22)
 (3.22)



297 **3.2. A third order semi-discrete scheme.** Similarly, we can extend the third
 298 order scheme to solve MBL equation (1.10), however, it is more involved. But
 299 the third order semi-discrete central scheme proposed in [12] can be extended to
 300 solve the MBL equation in a straightforward manner. In order to make the paper
 301 self-contained, we include the formulation below.

$$\frac{d\bar{w}_j}{dt} = -\frac{H_{j+1/2}(t) - H_{j-1/2}(t)}{\Delta x} + \epsilon Q_j(t)$$

302 where $\bar{w}(x, t)$ denotes the cell average of w

$$\bar{w}_j(t) = \frac{1}{\Delta x} \int_{x_{j-1/2}}^{x_{j+1/2}} w(x, t) dx,$$

303 $H_{j+1/2}(t)$ is the numerical convection flux and $Q_j(t)$ is a high-order approximation
 304 to the diffusion term u_{xx} .

$$H_{j+1/2}(t) = \frac{f(u_{j+1/2}^+(t)) + f(u_{j+1/2}^-(t))}{2} - \frac{a_{j+1/2}(t)}{2} [w_{j+1/2}^+(t) - w_{j+1/2}^-(t)]$$

where $u_{j+1/2}^-(t), u_{j+1/2}^+(t)$ denote the left and right intermediate values of $u(x, t^n)$
 at $x_{j+1/2}$, and their values are converted from the $w_{j+1/2}^-(t), w_{j+1/2}^+(t)$ using (3.2).
 The way to calculate $w_{j+1/2}^-(t), w_{j+1/2}^+(t)$ and $a_{j+1/2}(t)$ is

$$\begin{aligned} w_{j+1/2}^+(t) &= A_{j+1} - \frac{\Delta x}{2} B_{j+1} + \frac{(\Delta x)^2}{8} C_{j+1}, \\ w_{j+1/2}^-(t) &= A_j + \frac{\Delta x}{2} B_j + \frac{(\Delta x)^2}{8} C_j, \\ a_{j+1/2}(t) &= \max \left\{ \frac{\partial f}{\partial u}(u_{j+1/2}^-(t)), \frac{\partial f}{\partial u}(u_{j+1/2}^+(t)) \right\}, \end{aligned}$$

where

$$\begin{aligned}
A_j &= \bar{w}_j^n - \frac{w_C}{12}(\bar{w}_{j+1}^n - 2\bar{w}_j^n + \bar{w}_{j-1}^n), \\
B_j &= \frac{1}{\Delta x} \left[w_R(\bar{w}_{j+1}^n - \bar{w}_j^n) + w_C \frac{\bar{w}_{j+1}^n - \bar{w}_{j-1}^n}{2} + w_L(\bar{w}_j^n - \bar{w}_{j-1}^n) \right], \\
C_j &= 2w_C \frac{\bar{w}_{j-1}^n - 2\bar{w}_j^n + \bar{w}_{j+1}^n}{\Delta x^2}, \\
w_i &= \frac{\alpha_i}{\sum_m \alpha_m} \quad \alpha_i = \frac{c_i}{(\epsilon_0 + IS_i)^p}, \quad i, m \in \{C, R, L\} \\
c_L &= c_R = 1/4, \quad c_C = 1/2, \quad \epsilon_0 = 10^{-6}, \quad p = 2, \\
IS_L &= (\bar{w}_j^n - \bar{w}_{j-1}^n)^2, \quad IS_R = (\bar{w}_{j+1}^n - \bar{w}_j^n)^2, \\
IS_C &= \frac{13}{3}(\bar{w}_{j+1}^n - 2\bar{w}_j^n + \bar{w}_{j-1}^n)^2 + \frac{1}{4}(\bar{w}_{j+1}^n - \bar{w}_{j-1}^n)^2.
\end{aligned}$$

305 The diffusion u_{xx} is approximated using the following fourth-order central differ-
306 encing form

$$(3.23) \quad Q_j(t) = \frac{-u_{j-2} + 16u_{j-1} - 30u_j + 16u_{j+1} - u_{j+2}}{12\Delta x^2}.$$

307 The unique feature of this scheme is that the discretization is done in space first, and
308 then the time evolution equation can be solved as a system of ordinary differential
309 equations using any ODE solver of third order or higher. In this paper, we simply
310 use the standard fourth order Runge-Kutta methods. Notice that to achieve the
311 third order accuracy, the linear solver that converts u from w using (3.2) need also
312 to be high order, and (3.23) is used to discretize u_{xx} in our conversion.

313 4. COMPUTATIONAL RESULTS

314 In this section, we show the numerical solutions to the MBL equation

$$(4.1) \quad u_t + (f(u))_x = \epsilon u_{xx} + \epsilon^2 \tau u_{xxt}$$

315 with the initial condition

$$(4.2) \quad u_0(x) = \begin{cases} u_B & \text{if } x = 0 \\ 0 & \text{if } x > 0 \end{cases}$$

316 and the Dirichlet boundary condition.

317 Numerically, it is not practical to solve the half line problem (4.2), and one
318 has to choose an appropriate computational domain. Theorem 2.10 in Chapter 2
319 provides a theoretical bound for the difference between the solution to the half line
320 problem and that to the finite interval problem. However, the estimate (2.41) in
321 Theorem 2.10 includes time-dependent parameters $D_{1;\epsilon,\tau}(t)$ and $D_{2;\epsilon,\tau}(t)$, which
322 cannot be obtained analytically. Therefore, we numerically demonstrate how the
323 computational domain size affects the solution. We choose $\tau = 5$, $u_B = \alpha = \sqrt{\frac{2}{3}}$
324 and $\epsilon = 0.001$ as an example here. Figure 4.1 shows the snapshot of the solutions at
325 $t = 0.1$, $t = 0.5$ and $t = 1$ for computational domain $[0, L]$ with $L = 0.25$, $L = 0.75$
326 and $L = 1.25$.

327 In Figure 4.1(a), $t = 0.1$, the leading shock is located at $\frac{f(\bar{u}_{\tau=5})}{\bar{u}_{\tau=5}} \times 0.1 = 1.02 \times$
328 $0.1 = 0.102$, and $L = 0.25$, $L = 0.75$, $L = 1.25$ all exceed the leading shock location.
329 Hence all the three computational domains deliver visually indistinguishable results.
330 Whereas, in Figure 4.1(b), $t = 0.5$, the leading shock is located at $1.02 \times 0.5 = 0.51$,

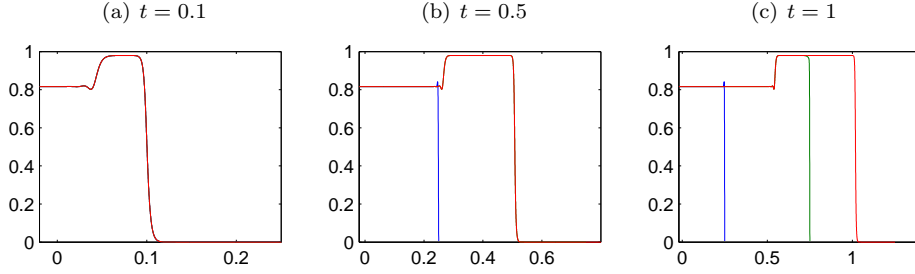


FIGURE 4.1. Numerical solutions of MBL (4.1) at (a) $t = 0.1$, (b) $t = 0.5$, (c) $t = 1$ using the trapezoid scheme (3.20). ‘—’, ‘—’, ‘—’ denote the numerical solutions corresponding to computational domain $[0, L]$ with $L = 0.25$, $L = 0.75$ and $L = 1.25$ respectively. The parameter values are $\tau = 5$, $u_B = \alpha = \sqrt{\frac{2}{3}}$, $\epsilon = 0.001$, $\Delta x = \frac{\epsilon}{10}$, $\Delta t = 0.1\Delta x$.

331 $L = 0.25$ is shorter than the computational domain needed to capture this shock,
 332 hence the numerical solution halts at $x = 0.25$. On the contrast, $L = 0.75$ and $L =$
 333 1.25 are both large enough to capture this shock front. Similarly, in Figure 4.1(c),
 334 $t = 1$, the leading shock is located at 1.02 . $L = 0.25 < 1.02$ and $L = 0.75 < 1.02$
 335 both result in wrong solution profiles. More specifically, both solutions halt at the
 336 boundary of the insufficient computational domain. But $L = 1.25 > 1.02$ is large
 337 enough to capture the correct solution profile.

In the rest of this chapter, all the computational domains $[0, L]$ are therefore chosen based on the principle:

$$L > \text{leading shock speed} \times \text{computational time.}$$

338 In addition, numerical solutions for larger L 's, for example, $L = 1.75$, $L = 2.5$,
 339 $L = 5$, $L = 10$ are also sought. For all these larger L 's, the numerical solutions
 340 are all consistent with that corresponding to $L = 1.25$ up to $t = 1$. This confirms
 341 that it is not necessary to take L too much larger than **leading shock speed** \times
 342 **computational time**.

343 To validate the order analysis given in chapter 3 for various schemes proposed,
 344 we first test the order of our schemes numerically with a smooth initial condition

$$u_0(x) = u_B H(x - 5, 5),$$

345 where

$$H(x, \xi) = \begin{cases} 1 & \text{if } x < -\xi \\ 1 - \frac{1}{2}(1 + \frac{x}{\xi} + \frac{1}{\pi} \sin(\frac{\pi x}{\xi})) & \text{if } -\xi \leq x \leq \xi \\ 0 & \text{if } x > \xi \end{cases} .$$

346 The final time $T = 1$ was employed, so that there was no shock created. ϵ in the
 347 MBL equation (4.1) is taken to be 1, M is taken to be 2, and the computational
 348 interval is $[-10, 20]$. The L_1, L_2, L_∞ order tests of the trapezoid scheme and the
 349 third order semi-discrete scheme with different parameter τ value and the initial
 350 condition u_B are given in Tables 4.1, 4.2. Table 4.1 shows that the trapezoid rule
 351 achieved second order accuracy for all the tested cases in L_1, L_2, L_∞ sense. Table

	N	$\ u_{\Delta x} - u_{\frac{\Delta x}{2}}\ _1$ order		$\ u_{\Delta x} - u_{\frac{\Delta x}{2}}\ _2$ order		$\ u_{\Delta x} - u_{\frac{\Delta x}{2}}\ _\infty$ order	
$u_B = 0.9$ $\tau = 0.2$	60	7.5416e-03	-	2.5388e-03	-	1.5960e-03	-
	120	1.9684e-03	1.9379	6.7288e-04	1.9157	4.4066e-04	1.8568
	240	4.9891e-04	1.9802	1.7645e-04	1.9311	1.2529e-04	1.8144
	480	1.2589e-04	1.9865	4.5366e-05	1.9596	3.3205e-05	1.9158
$u_B = 0.9$ $\tau = 1$	60	8.0141e-03	-	2.6069e-03	-	1.4989e-03	-
	120	2.1502e-03	1.8981	7.0452e-04	1.8876	4.2221e-04	1.8279
	240	5.5697e-04	1.9488	1.8259e-04	1.9480	1.1283e-04	1.9038
	480	1.4104e-04	1.9815	4.6109e-05	1.9855	2.8719e-05	1.9740
$u_B = 0.9$ $\tau = 5$	60	1.3102e-02	-	4.1784e-03	-	2.2411e-03	-
	120	3.6201e-03	1.8557	1.0994e-03	1.9263	6.1060e-04	1.8759
	240	9.6737e-04	1.9039	2.8089e-04	1.9686	1.5667e-04	1.9625
	480	2.5825e-04	1.9053	7.1250e-05	1.9790	3.9286e-05	1.9956
$u_B = \alpha$ $\tau = 0.2$	60	6.4427e-03	-	2.1578e-03	-	1.1682e-03	-
	120	1.6611e-03	1.9555	5.7775e-04	1.9011	3.6447e-04	1.6804
	240	4.3643e-04	1.9283	1.5215e-04	1.9250	1.0389e-04	1.8107
	480	1.1223e-04	1.9593	3.9170e-05	1.9577	2.7629e-05	1.9109
$u_B = \alpha$ $\tau = 1$	60	7.5867e-03	-	2.4101e-03	-	1.3364e-03	-
	120	2.0069e-03	1.9185	6.4998e-04	1.8906	3.7650e-04	1.8277
	240	5.1832e-04	1.9531	1.6801e-04	1.9519	1.0062e-04	1.9037
	480	1.3136e-04	1.9803	4.2497e-05	1.9831	2.5599e-05	1.9748
$u_B = \alpha$ $\tau = 5$	60	1.1959e-02	-	3.8026e-03	-	1.9938e-03	-
	120	3.2940e-03	1.8602	9.9527e-04	1.9338	5.4231e-04	1.8783
	240	8.7736e-04	1.9086	2.5358e-04	1.9727	1.3933e-04	1.9606
	480	2.3271e-04	1.9146	6.4252e-05	1.9806	3.4967e-05	1.9944
$u_B = 0.75$ $\tau = 0.2$	60	5.7714e-03	-	1.9358e-03	-	1.0481e-03	-
	120	1.5035e-03	1.9406	5.1617e-04	1.9070	2.8061e-04	1.9011
	240	3.9299e-04	1.9357	1.3616e-04	1.9225	7.9134e-05	1.8262
	480	1.0063e-04	1.9655	3.5080e-05	1.9566	2.1035e-05	1.9115
$u_B = 0.75$ $\tau = 1$	60	7.1823e-03	-	2.2843e-03	-	1.2069e-03	-
	120	1.8963e-03	1.9213	6.1315e-04	1.8974	3.4013e-04	1.8272
	240	4.8284e-04	1.9736	1.5796e-04	1.9567	9.0912e-05	1.9035
	480	1.2093e-04	1.9974	3.9783e-05	1.9894	2.3121e-05	1.9753
$u_B = 0.75$ $\tau = 5$	60	1.1042e-02	-	3.5020e-03	-	1.8299e-03	-
	120	3.0287e-03	1.8662	9.1181e-04	1.9414	4.8976e-04	1.9016
	240	8.0111e-04	1.9186	2.3118e-04	1.9797	1.2593e-04	1.9595
	480	2.1076e-04	1.9264	5.8358e-05	1.9860	3.1627e-05	1.9934

TABLE 4.1. The accuracy test for the trapezoid scheme for the MBL equation (4.1) with $\epsilon = 1$ and $M = 2$.

352 4.2 shows that the semi-discrete scheme has the order of accuracy greater than 2.5
353 for all the cases, and exceeds 3 for some cases. This confirms the accuracy study
354 given in sections 3.1.1 and 3.2 respectively.

355 We will now use examples to study the solutions to MBL equation (4.1) using
356 the numerical schemes proposed in chapter 3. We first notice that if we scale t and
357 x as follows

$$\tilde{t} = \frac{t}{\epsilon}, \quad \tilde{x} = \frac{x}{\epsilon},$$

358 then MBL (4.1) equation can be written in terms of \tilde{t} and \tilde{x} as follows

$$(4.3) \quad u_{\tilde{t}} + (f(u))_{\tilde{x}} = u_{\tilde{x}\tilde{x}} + \tau u_{\tilde{x}\tilde{t}\tilde{t}}.$$

	N	$\ u_{\Delta x} - u_{\frac{\Delta x}{2}}\ _1$ order		$\ u_{\Delta x} - u_{\frac{\Delta x}{2}}\ _2$ order		$\ u_{\Delta x} - u_{\frac{\Delta x}{2}}\ _\infty$ order	
$u_B = 0.9$ $\tau = 0.2$	120	2.6992e-03	-	1.1300e-03	-	7.2363e-04	-
	240	4.0403e-04	2.7400	1.7079e-04	2.7260	1.1283e-04	2.6811
	480	5.7504e-05	2.8127	2.4624e-05	2.7941	1.6242e-05	2.7963
	960	8.4934e-06	2.7592	3.0892e-06	2.9948	1.7607e-06	3.2055
$u_B = 0.9$ $\tau = 1$	120	4.7731e-03	-	2.0192e-03	-	1.7267e-03	-
	240	8.7205e-04	2.4524	3.6879e-04	2.4529	3.0632e-04	2.4949
	480	1.2006e-04	2.8606	5.0480e-05	2.8690	4.1985e-05	2.8671
	960	1.5942e-05	2.9129	6.6663e-06	2.9208	5.1464e-06	3.0282
$u_B = 0.9$ $\tau = 5$	120	3.7573e-03	-	1.2122e-03	-	7.9211e-04	-
	240	7.4624e-04	2.3320	2.4164e-04	2.3267	1.5061e-04	2.3949
	480	1.1994e-04	2.6373	3.8434e-05	2.6524	2.5089e-05	2.5857
	960	1.5565e-05	2.9460	4.9190e-06	2.9660	3.1363e-06	2.9999
$u_B = \alpha$ $\tau = 0.2$	120	2.1836e-03	-	9.1039e-04	-	5.7219e-04	-
	240	3.2729e-04	2.7381	1.3760e-04	2.7260	8.9550e-05	2.6757
	480	4.6856e-05	2.8043	1.9909e-05	2.7890	1.2935e-05	2.7914
	960	6.7382e-06	2.7978	2.3182e-06	3.1023	1.4109e-06	3.1965
$u_B = \alpha$ $\tau = 1$	120	3.9014e-03	-	1.6388e-03	-	1.3873e-03	-
	240	7.0517e-04	2.4680	2.9669e-04	2.4656	2.4272e-04	2.5149
	480	9.6528e-05	2.8690	4.0354e-05	2.8781	3.3125e-05	2.8733
	960	1.2890e-05	2.9047	5.3648e-06	2.9111	4.0754e-06	3.0229
$u_B = \alpha$ $\tau = 5$	120	3.0797e-03	-	9.9202e-04	-	6.4456e-04	-
	240	6.1133e-04	2.3328	1.9783e-04	2.3261	1.2277e-04	2.3924
	480	9.7351e-05	2.6507	3.1222e-05	2.6637	2.0263e-05	2.5990
	960	1.2396e-05	2.9733	3.9513e-06	2.9822	2.4962e-06	3.0210
$u_B = 0.75$ $\tau = 0.2$	120	1.8244e-03	-	7.5548e-04	-	4.6671e-04	-
	240	2.7262e-04	2.7425	1.1419e-04	2.7260	7.3299e-05	2.6707
	480	3.9198e-05	2.7980	1.6562e-05	2.7855	1.0681e-05	2.7788
	960	5.4739e-06	2.8401	1.9677e-06	3.0733	1.3232e-06	3.0129
$u_B = 0.75$ $\tau = 1$	120	3.2727e-03	-	1.3672e-03	-	1.1477e-03	-
	240	5.8671e-04	2.4798	2.4585e-04	2.4754	1.9866e-04	2.5304
	480	7.9974e-05	2.8750	3.3285e-05	2.8848	2.7033e-05	2.8775
	960	1.0724e-05	2.8987	4.4466e-06	2.9041	3.3341e-06	3.0193
$u_B = 0.75$ $\tau = 5$	120	2.5902e-03	-	8.3335e-04	-	5.3882e-04	-
	240	5.1342e-04	2.3348	1.6611e-04	2.3268	1.0271e-04	2.3913
	480	8.1062e-05	2.6630	2.6032e-05	2.6738	1.6813e-05	2.6109
	960	1.0173e-05	2.9944	3.2662e-06	2.9946	2.0473e-06	3.0377

TABLE 4.2. The accuracy test for the third order semi-discrete scheme for the MBL equation (4.1) with $\epsilon = 1$ and $M = 2$.

359 The scaled equation (4.3) shows that it is the magnitude of $\frac{t}{\epsilon}$ and $\frac{x}{\epsilon}$ that determine
360 the asymptotic behavior, not t , x , neither ϵ alone ([21]). In addition, (4.3) also shows
361 that the dispersive parameter τ denotes the relative importance of the dispersive
362 term u_{xxt} . The bigger τ is, the more dispersive effect (4.1) equation has. This can
363 be seen from the computational results to be shown later in this section.

364 Duijn et al. [21] numerically provided a bifurcation diagram (Figure 4.2) of MBL
365 (4.1) equation as the dispersive parameter τ and the post-shock value u_B of the
366 initial condition vary. The solution of (4.1) has been proven to display qualitatively
367 different profiles for parameter values (τ, u_B) falling in different regimes of the
368 bifurcation diagram. In particular, for every fixed τ value, there are two critical

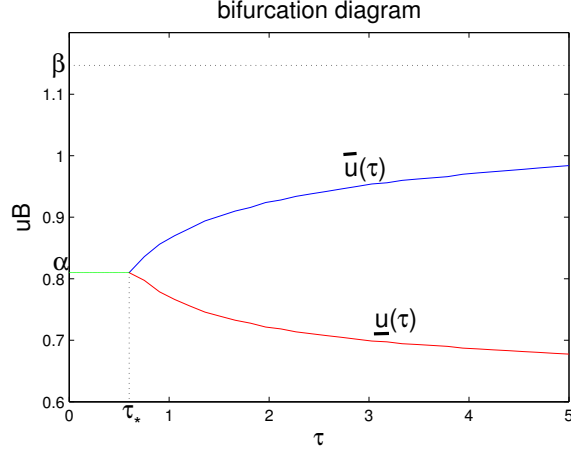


FIGURE 4.2. The bifurcation diagram of the MBL equation (1.10) with the bifurcation parameters (τ, u_B) .

369 u_B values, namely, \bar{u} and \underline{u} . From the bifurcation diagram (Figure 4.2), it is clear
 370 that, when $\tau < \tau_*$, $\bar{u} = \underline{u} = \alpha$. For a fixed τ value, the solution has three different
 371 profiles.

- 372 (a) If $u_B \in [\bar{u}, 1]$, the solution contains a plateau value u_B for $0 \leq \frac{x}{t} \leq \frac{df}{du}(u_B)$,
 373 a rarefaction wave connection u_B to \bar{u} for $\frac{df}{du}(u_B) \leq \frac{x}{t} \leq \frac{df}{du}(\bar{u})$, another
 374 plateau value \bar{u} for $\frac{df}{du}(\bar{u}) < \frac{x}{t} < \frac{f(\bar{u})}{\bar{u}}$, and a shock from \bar{u} down to 0 at
 375 $\frac{x}{t} = \frac{f(\bar{u})}{\bar{u}}$ (see Figure 3(a)).
 376 (b) If $u_B \in (\underline{u}, \bar{u})$, the solution contains a plateau value u_B for $0 \leq \frac{x}{t} <$
 377 $\frac{f(\bar{u})-f(u_B)}{\bar{u}-u_B}$, a shock from u_B up to \bar{u} at $\frac{x}{t} = \frac{f(\bar{u})-f(u_B)}{\bar{u}-u_B}$, another plateau
 378 value \bar{u} for $\frac{f(\bar{u})-f(u_B)}{\bar{u}-u_B} < \frac{x}{t} < \frac{f(\bar{u})}{\bar{u}}$, and a shock from \bar{u} down to 0 at
 379 $\frac{x}{t} = \frac{f(\bar{u})}{\bar{u}}$ (see Figure 3(b)). The solution may exhibit a damped oscillation
 380 near $u = u_B$.
 381 (c) If $u_B \in (0, \underline{u}]$, the solution consists a single shock connecting u_B and 0
 382 at $\frac{x}{t} = \frac{f(u_B)}{u_B}$ (see Figure 3(c)). It may exhibit oscillatory behavior near
 383 $u = u_B$.

384 Notice that when $\tau > \tau_*$ and $\underline{u} < u_B < \bar{u}$, the solution profiles (3(b)) displays
 385 non-monotonicity, which is consistent with the experimental observations ([7]).

386 In the numerical computation we show below, we will therefore test the accuracy
 387 and capability of central schemes for different parameter values (τ and u_B) that fall
 388 into various regimes of the bifurcation diagram, and therefore display qualitatively
 389 different solution profiles. The numerical experiments were carried out for $M = 2$,
 390 $\epsilon = 0.001$ and $T = 4000 \times \epsilon$, i.e. $\bar{T} = 4000$ to get the asymptotic solution profiles,
 391 and Δx was chosen to be $\frac{\epsilon}{10}$ and $\lambda = \frac{\Delta t}{\Delta x}$ was chosen to be 0.1. The scheme used
 392 in the computation is the second order Trapezoid scheme as shown in section 3.1.1.
 393 The Midpoint scheme delivers similar computational results, hence is omitted here.
 394 The solution profiles at $\frac{T}{4}$ (blue), $\frac{2*T}{4}$ (green), $\frac{3*T}{4}$ (magenta) and T (black) are

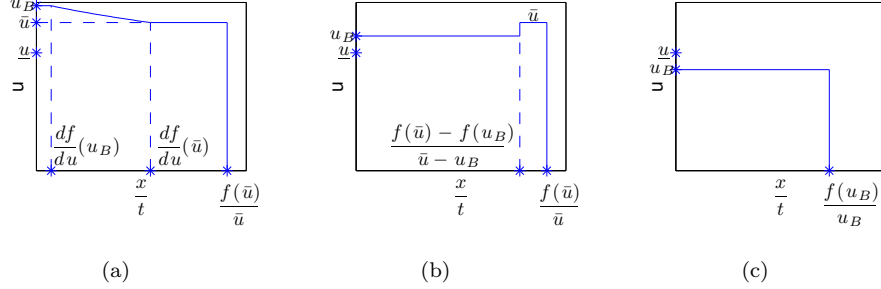


FIGURE 4.3. Given a fixed τ , the three qualitatively different solution profiles due to different values of u_B . In particular, when $\tau > \tau_*$ and $\underline{u} < u_B < \bar{u}$, the solution profiles (Figure 3(b)) displays non-monotonicity, which is consistent with the experimental observations ([7]). Figures 3(a), 3(b) and 3(c) are demonstrative figures.

395 chosen to demonstrate the time evolution of the solutions. The red dashed lines are
 396 used to denote the theoretical shock locations and plateau values for comparison
 397 purpose.

398 We start with $\tau > 0$. Based on the bifurcation diagram (Figure 4.2), we choose
 399 three representative u_B values, i.e. $u_B = 0.9 > \alpha$, $u_B = \alpha = \sqrt{\frac{M}{M+1}} = \sqrt{\frac{2}{3}}$ (for
 400 $M = 2$) and $u_B = 0.75 < \alpha$. For each fixed u_B , we choose three representative τ
 401 values, i.e. $\tau = 0.2 < \tau_* \approx 0.61$, $\tau = 1 > \tau_*$ with $u_B = 0.75 < \underline{u}_{\tau=1} < u_B = \alpha <$
 402 $\bar{u} < u_B = 0.9$, and $\tau = 5$ with $u_B = 0.75, \alpha, 0.9 \in [\underline{u}_{\tau=5}, \bar{u}_{\tau=5}]$. We first use this 9
 403 pairs of (τ, u_B) values given in Table 4.3 to validate the solution profiles with the
 demonstrative solution profiles given in Figure 4.3.

(τ, u_B)	Example 4	Example 5	Example 6
Example 1	(0.2, 0.9)	(1, 0.9)	(5, 0.9)
Example 2	(0.2, α)	(1, α)	(5, α)
Example 3	(0.2, 0.75)	(1, 0.75)	(5, 0.75)

TABLE 4.3. 9 pairs of (τ, u_B) values with either fixed τ value or fixed u_B value used in Examples 1 – 6.

404

405 **Example 1** $(\tau, u_B) = (0.2, 0.9), (\tau, u_B) = (1, 0.9), (\tau, u_B) = (5, 0.9)$.

406 When $u_B = 0.9 > \alpha$ is fixed, we increase τ from 0.2 to 1 to 5 (Figure 4(a) , 4(b)
 407 , 4(c)), the dispersive effect starts to dominate the solution profile. When $\tau = 0.2$
 408 (Figure 4(a)), the solution profile is similar to the classical BL equation solution
 409 (see Figure 2(b)), with a rarefaction wave for $\frac{x}{t} \in [f'(u = 0.9), f'(u = \alpha) = f'(u =$
 410 $\bar{u}_{\tau=0.2})]$ and a shock from $u = \alpha$ to $u = 0$ at $\frac{x}{t} = f'(\alpha)$. This corresponds to
 411 Figure 3(a) with $\frac{df}{du}(\bar{u}_{\tau=0.2} = \alpha) = \frac{f(\bar{u}_{\tau=0.2})}{\bar{u}_{\tau=0.2}} = \frac{f(\alpha)}{\alpha}$. When $\tau = 1$ (Figure 4(b)),
 412 the rarefaction wave is between $\frac{x}{t} \in [f'(u = 0.9), f'(u = \bar{u}_{\tau=1})]$ and the solution
 413 remains at the plateau value $u = \bar{u}_{\tau=1}$ for $\frac{x}{t} \in [f'(u = \bar{u}_{\tau=1}), \frac{f(\bar{u}_{\tau=1})}{\bar{u}_{\tau=1}}]$ and the shock

414 occurs at $\frac{x}{t} = \frac{f(\bar{u}_{\tau=1})}{\bar{u}_{\tau=1}}$. This corresponds to Figure 3(a) with $u_B = 0.9 > \bar{u}_{\tau=1} \approx$
 415 0.86 . When $\tau = 5$ (Figure 4(c)), the solution displays the first shock from $u = 0.9$
 416 to $u = \bar{u}_{\tau=5}$ at $\frac{x}{t} = \frac{f(\bar{u}_{\tau=5}) - f(u_B)}{\bar{u}_{\tau=5} - u_B}$, and then remains at the plateau value $u = \bar{u}_{\tau=5}$
 417 for $\frac{x}{t} \in [\frac{f(\bar{u}_{\tau=5}) - f(u_B)}{\bar{u}_{\tau=5} - u_B}, \frac{f(\bar{u}_{\tau=5})}{\bar{u}_{\tau=5}}]$ and the second shocks occurs at $\frac{x}{t} = \frac{f(\bar{u}_{\tau=5})}{\bar{u}_{\tau=5}}$. This
 418 corresponds to Figure 3(b) with $\underline{u}_{\tau=5} \approx 0.68 < u_B = 0.9 < \bar{u}_{\tau=5} \approx 0.98$. Notice
 419 that as τ increases, the rarefaction region shrinks and the plateau region enlarges.

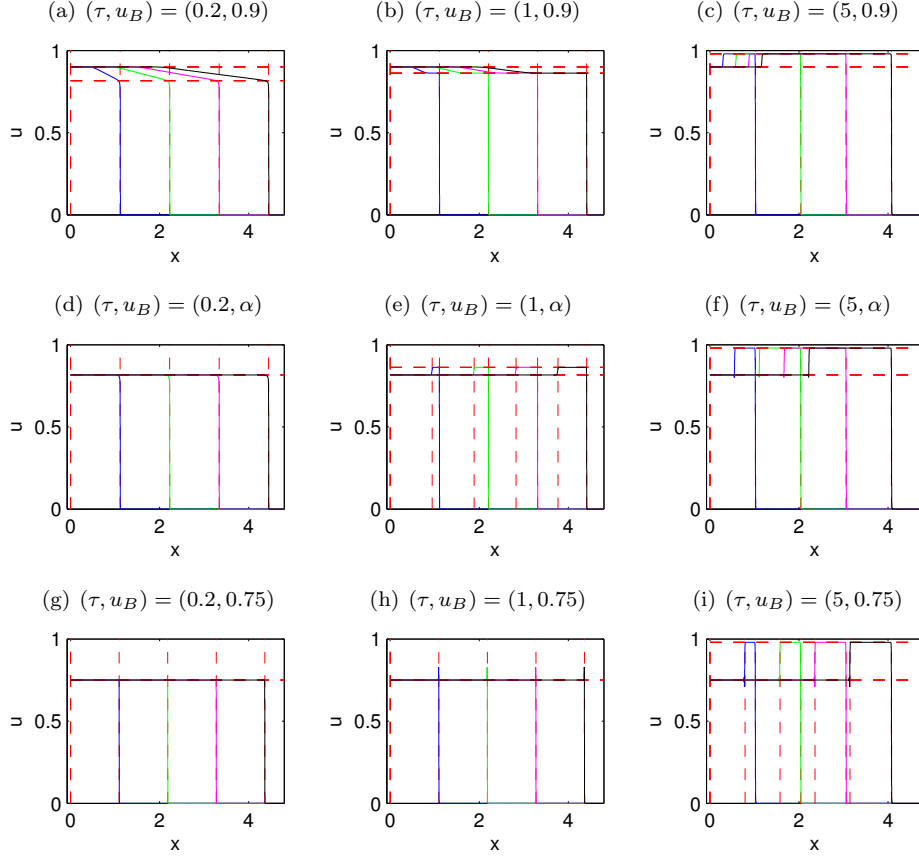


FIGURE 4.4. Numerical solutions to MBL equation with parameter settings fall in different regimes of the bifurcation diagram (Figure 4.2). The color coding is for different time: $\frac{1}{4}T$ (blue), $\frac{2}{4}T$ (green), $\frac{3}{4}T$ (magenta) and T (black). The results are discussed in examples 1 – 6. In figures 4(d) – 4(f), $\alpha = \sqrt{\frac{M}{M+1}} = \sqrt{\frac{2}{3}}$ for $M = 2$.

420

421 **Example 2** $(\tau, u_B) = (0.2, \alpha), (\tau, u_B) = (1, \alpha), (\tau, u_B) = (5, \alpha)$.

422 When $u_B = \alpha$ is fixed, we increase τ from 0.2 to 1 to 5 (Figure 4(d) , 4(e) , 4(f)),
 423 the dispersive effect starts to dominate the solution profile. When $\tau = 0.2$, the
 424 solution displays one single shock at $\frac{x}{t} = \frac{f(\alpha)}{\alpha}$. For both $\tau = 1$ and $\tau = 5$, the

425 solution has two shocks, one at $\frac{x}{t} = \frac{f(\bar{u}_{\tau=1(\tau=5 \text{ respectively})}) - f(\alpha)}{\bar{u}_{\tau=1(\tau=5 \text{ respectively})} - \alpha}$, and another one
 426 at $\frac{x}{t} = \frac{f(\bar{u}_{\tau=1(\tau=5 \text{ respectively})})}{\bar{u}_{\tau=1(\tau=5 \text{ respectively})}}$. For both $\tau = 1$ and $\tau = 5$ (Figures 4(e) 4(f)), the
 427 solutions correspond to Figure 3(b), which are consistent to the experimental obser-
 428 vations. Notice that as τ increases from 1 to 5, i.e., the dispersive effect increases,
 429 the inter-shock interval length increases at every fixed time (compare Figure 4(e)
 430 with Figure 4(f)). In addition, for fix $\tau = 1$ ($\tau = 5$ respectively), as time progresses,
 431 the inter-shock interval length increases in the linear fashion (see Figure 4(e) (Fig-
 432 ure 4(f) respectively)).

433
 434 **Example 3** $(\tau, u_B) = (0.2, 0.75), (\tau, u_B) = (1, 0.75), (\tau, u_B) = (5, 0.75)$.
 435 When $u_B = 0.75 \leq \alpha$ is fixed, we increase τ from 0.2 to 1 to 5 (Figure 4(g) , 4(h)
 436 , 4(i)), the dispersive effects starts to dominate the solution profile in the similar
 437 fashion as $u_B = 0.9$ and $u_B = \alpha$. Notice that when $\tau = 1$, since $u_B = 0.75$ is
 438 very close to $\underline{u}_{\tau=1}$, the solution displays oscillation at $\frac{x}{t} = \frac{f(u_B)}{u_B}$ (Figure 4(h)). If
 439 we increase τ further to $\tau = 5$, the dispersive effect is strong enough to create a
 440 plateau value at $\bar{u} \approx 0.98$ (see Figure 4(i)).

441
 442 **Example 4** $(\tau, u_B) = (0.2, 0.9), (\tau, u_B) = (0.2, \alpha), (\tau, u_B) = (0.2, 0.75)$.
 443 Now, we fix $\tau = 0.2$, decrease u_B from 0.9 to α , to 0.75 (Figures 4(a) 4(d) 4(g)). If
 444 $u_B > \alpha$ the solution consists a rarefaction wave connecting u_B down to α , then a
 445 shock from α to 0, otherwise, the solution consists a single shock from u_B down to
 446 0. In all cases, since $\tau = 0.2 < \tau_*$, regardless of the u_B value, the solution will not
 447 display non-monotone behavior, due to the lack of dispersive effect.

448
 449 **Example 5** $(\tau, u_B) = (1, 0.9), (\tau, u_B) = (1, \alpha), (\tau, u_B) = (1, 0.75)$.
 450 Now, we fix $\tau = 1$, decrease u_B from 0.9 to α , to 0.75 (Figures 4(b) 4(e) 4(h)). If
 451 $u_B = 0.9 > \bar{u}_{\tau=1}$, the solution consists a rarefaction wave connecting u_B and \bar{u} ,
 452 and a shock connecting \bar{u} down to 0 (Figure 4(b)). Even if $\underline{u} < u_B < \bar{u}$, because
 453 $\tau = 1 > \tau_*$, the solution still has a chance to increase to the plateau value \bar{u} as seen
 454 in Figure 4(e). But, if u_B is too small, for example, $u_B = 0.75 < \underline{u}$, the solution
 455 does not increase to \bar{u} any more, instead, it consists a single shock connecting u_B
 456 down to 0 (Figure 4(h)).

457
 458 **Example 6** $(\tau, u_B) = (5, 0.9), (\tau, u_B) = (5, \alpha), (\tau, u_B) = (5, 0.75)$.
 459 Now, we fix $\tau = 5$, decrease u_B from 0.9 to α , to 0.75 (Figures 4(c) 4(f) 4(i)). For all
 460 three u_B , they are between $\underline{u}_{\tau=5}$ and $\bar{u}_{\tau=5}$, hence all increase to the plateau value
 461 $\bar{u}_{\tau=5} \approx 0.98$ before dropping to 0. Notice that as u_B decreases, the inter-shock
 462 interval length decreases at every fixed time (compare Figures 4(c), 4(f) and 4(i)).
 463 This shows that when the dispersive effect is strong ($\tau > \tau_*$), the bigger u_B is, the
 464 bigger region the solution stays at the plateau value.

465
 466 **Example 7** $(\tau, u_B) = (0, 0.9), (\tau, u_B) = (0, \alpha), (\tau, u_B) = (0, 0.75)$.
 467 We now show the solution profiles for the extreme τ value, i.e. $\tau = 0$ in Figures
 468 5(a) ($u_B = 0.9$), 5(b) ($u_B = \alpha$) and 5(c) ($u_B = 0.75$). Notice that these are cases
 469 of classical BL equation with small diffusion ϵu_{xx} . We compare Figures 5(a), 5(b)
 470 and 5(c) with the solution of the classical BL equation given in Figures 2(a) and
 471 2(b), it is clear that they show qualitatively same solution profiles. The difference

472 is that due to the diffusion term in the MBL equation, as shown in Figure 4.5, the
 473 solutions do not have sharp edges right at the shock, instead, the solutions smear
 474 out a little. If we compare Figures 5(a), 5(b) and 5(c) with Figures 4(a), 4(d) and
 475 4(g), there is no visible difference. This shows that once $\tau < \tau_*$, solution profile
 476 will stay the same for a fixed u_B value.

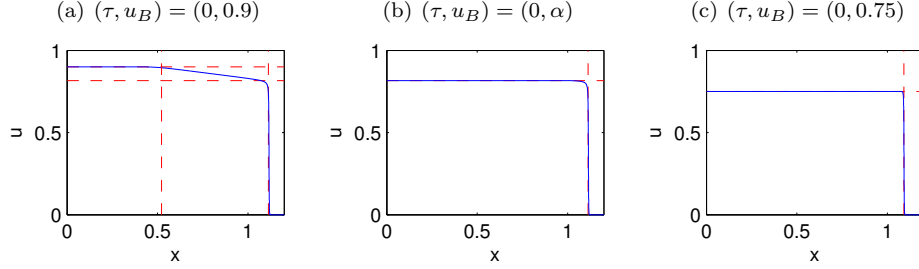


FIGURE 4.5. The numerical solutions of the MBL equation at $T = 1$ with $\tau = 0$ and different u_B values. The results are discussed in example 7.

477

478 **Example 8** $(\tau, u_B) = (5, 0.99)$, $(\tau, u_B) = (5, 0.98)$, $(\tau, u_B) = (5, 0.97)$.

479 We also study the solution profiles for u_B close to \bar{u} . For example, when $\tau = 5$,
 480 $\bar{u} \approx 0.98$, we hence choose $u_B = 0.99$, $u_B = 0.98$, $u_B = 0.97$ and solutions are
 481 shown in Figure 6(a), 6(b), 6(c). If $u_B = 0.99 > \bar{u}_{\tau=5} \approx 0.98$, the solution drops
 482 to the plateau value \bar{u} , then drops to 0 (see Figure 6(a)). If $u_B = 0.98 \approx \bar{u}_{\tau=5}$,
 483 the solution remains at plateau value $\bar{u}_{\tau=5}$ and then drop to 0 (see Figure 6(b)).
 484 If $u_B = 0.97 < \bar{u}_{\tau=5}$, the solution increases to the plateau value $\bar{u}_{\tau=5} \approx 0.98$, then
 485 drops to 0. In all cases, the transition from u_B to $\bar{u}_{\tau=5} \approx 0.98$ takes very small
 486 space. In the majority space, the solution keeps to be the plateau value $\bar{u}_{\tau=5} \approx 0.98$.

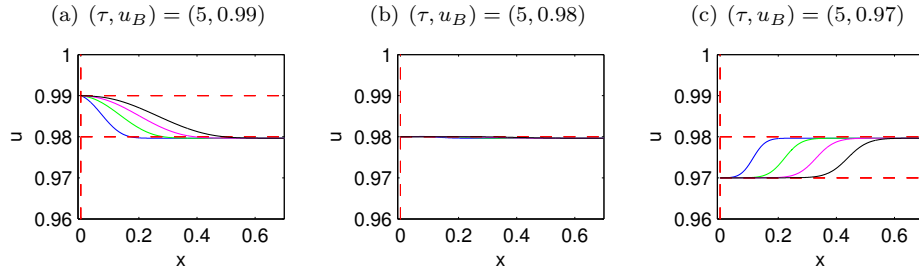


FIGURE 4.6. Numerical solutions to MBL equation with u_B close to $\bar{u}_{\tau=5} \approx 0.98$. The color coding is for different time: $\frac{1}{4}T$ (blue), $\frac{2}{4}T$ (green), $\frac{3}{4}T$ (magenta) and T (black). The results are discussed in example 8.

487

488 **Example 9** $(\tau, u_B) = (5, 0.7)$, $(\tau, u_B) = (5, 0.69)$, $(\tau, u_B) = (5, 0.68)$, $(\tau, u_B) =$
 489 $(5, 0.67)$, $(\tau, u_B) = (5, 0.66)$.

490 In addition, we study the solution profiles for u_B close to \underline{u} . For example, when
 491 $\tau = 5$, $\underline{u} \approx 0.68$, we hence choose $u_B = 0.7$, $u_B = 0.69$, $u_B = 0.68$, $u_B = 0.67$,
 492 $u_B = 0.66$ and solutions are shown in Figures 7(a), 7(b), 7(c), 7(d), 7(e). As
 493 u_B decreases crossing $\underline{u}_{\tau=5} \approx 0.68$, the solution gradually stops increasing to the
 494 plateau value $\bar{u}_{\tau=5}$, and the inter-shock interval length decreases (compare Figures
 495 7(a), 7(b) and 7(c)). The oscillation in Figures 7(d) and 7(e) are due to the fact
 496 that u_B values are too close to $\underline{u}_{\tau=5}$. This confirms that even with big dispersive
 497 effect (say $\tau = 5$), if u_B is too small (e.g. $u_B < \underline{u}$), the solution will not exhibit
 498 non-monotone behavior.

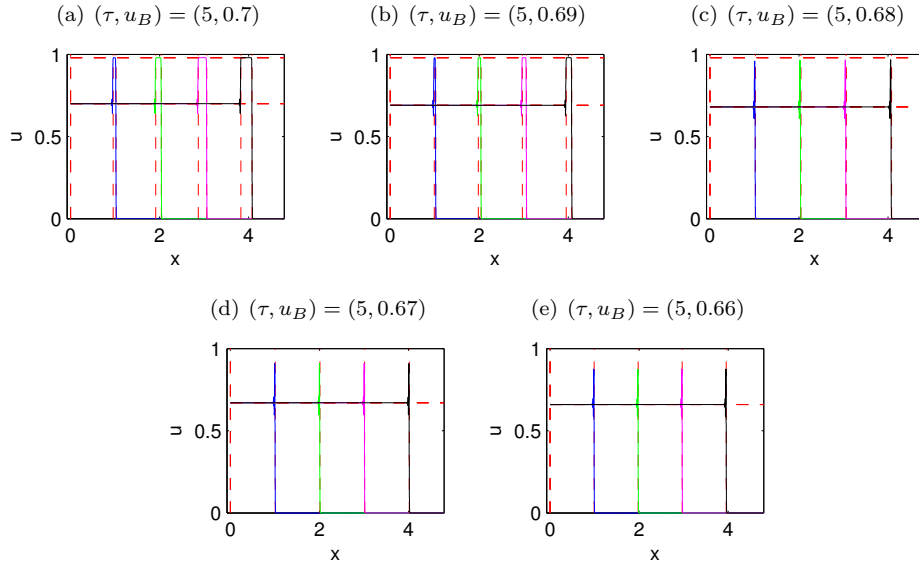


FIGURE 4.7. Numerical solutions to MBL equation with u_B close to $\underline{u}_{\tau=5} \approx 0.68$. The color coding is for different time: $\frac{1}{4}T$ (blue), $\frac{2}{4}T$ (green), $\frac{3}{4}T$ (magenta) and T (black). The results are discussed in example 9.

499

500 **Example 10** $(\tau, u_B) = (0.2, 0.6)$, $(\tau, u_B) = (1, 0.6)$, $(\tau, u_B) = (5, 0.6)$.

501 We fix u_B to be small, and in this example, we take it to be $u_B = 0.6$. We vary the τ
 502 value, from $\tau = 0.2 < \tau_*$ to $\tau = 1$ barely larger than τ_* to $\tau = 5 > \tau_*$. The numerical
 503 solutions are given in Figure 8(a), 8(b), 8(c). As τ increases, the post-shock value
 504 remains the same, but there will be oscillation generated as τ becomes larger than
 505 τ_* . Figures 8(d), 8(e) and 8(f) show that as τ increases, the oscillation amplitude
 506 increases and oscillates more rounds. Notice that τ is the dispersive parameter, and
 507 this means that even for small u_B value, different dispersive parameter values still
 508 give different dispersive effects, although none can bring the solution to the plateau
 509 value \bar{u} . Comparing Figures 8(d), 8(e) and 8(f) with Figures 8(g), 8(h) and 8(i), it
 510 is clear that the oscillation amplitude remains steady with respect to time.

511

512 **Example 11** $\epsilon = 0.001$, $\epsilon = 0.002$, $\epsilon = 0.003$, $\epsilon = 0.004$, $\epsilon = 0.005$.

513 In this example, we will compare the solution profiles for different ϵ values. Fixing

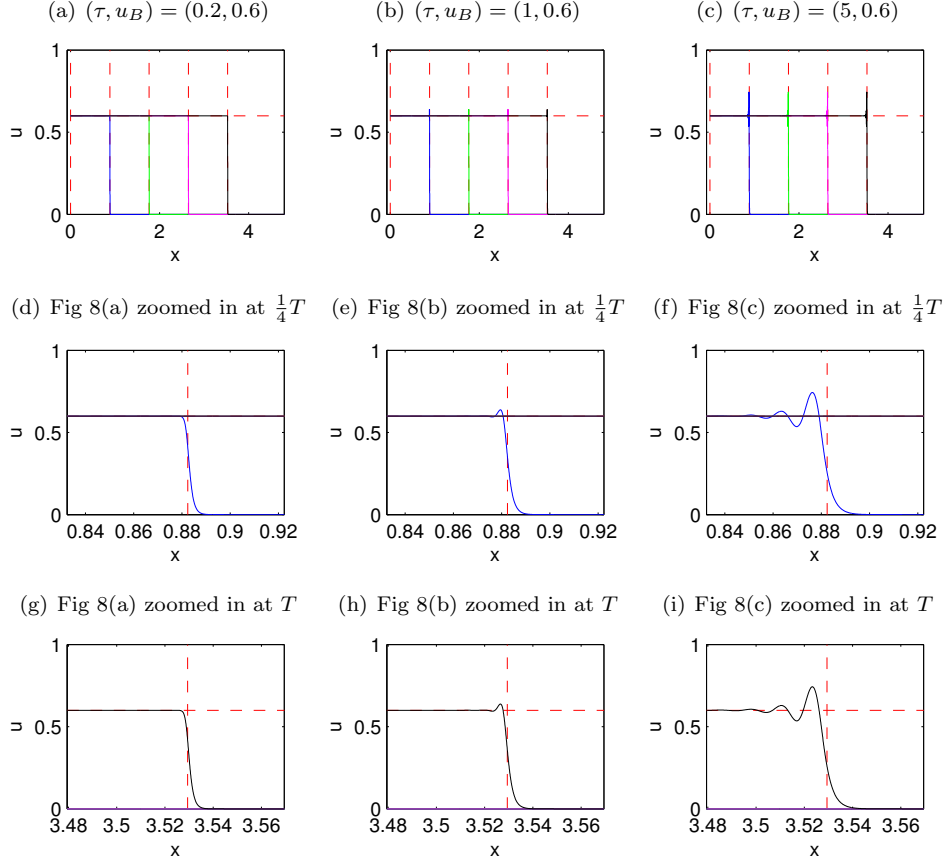


FIGURE 4.8. Numerical solutions to MBL equation with small constant $u_B = 0.6$ and different τ values. The figures on the second and third rows are the magnified versions of the first row at $t = \frac{1}{4}T$ and $t = T$ respectively. The color coding is for different time: $\frac{1}{4}T$ (blue), $\frac{2}{4}T$ (green), $\frac{3}{4}T$ (magenta) and T (black). The results are discussed in examples 10.

514 $T = 0.5, \Delta x = 0.0001, \lambda = \frac{\Delta t}{\Delta x} = 0.1$, we show the numerical results in Figure 4.9
 515 for $\epsilon = 0.001$ (blue), $\epsilon = 0.002$ (yellow), $\epsilon = 0.003$ (magenta), $\epsilon = 0.004$ (green),
 516 and $\epsilon = 0.005$ (black). For the purpose of cross reference, we choose the same
 517 nine sets of parameter settings as in examples 1– 6. To assist the observation, the
 518 figures in Figure 4.9 are zoomed into the regions where different ϵ values introduce
 519 different solution profiles. The numerical solutions clearly show that as ϵ increases,
 520 the numerical solution is smeared out, and the jump location becomes less accurate.
 521 Notice that τ is responsible for the competition between the diffusion and disper-
 522 sion, which in turn determines the plateau values. Hence varying ϵ value doesn't
 523 affect the plateau location.

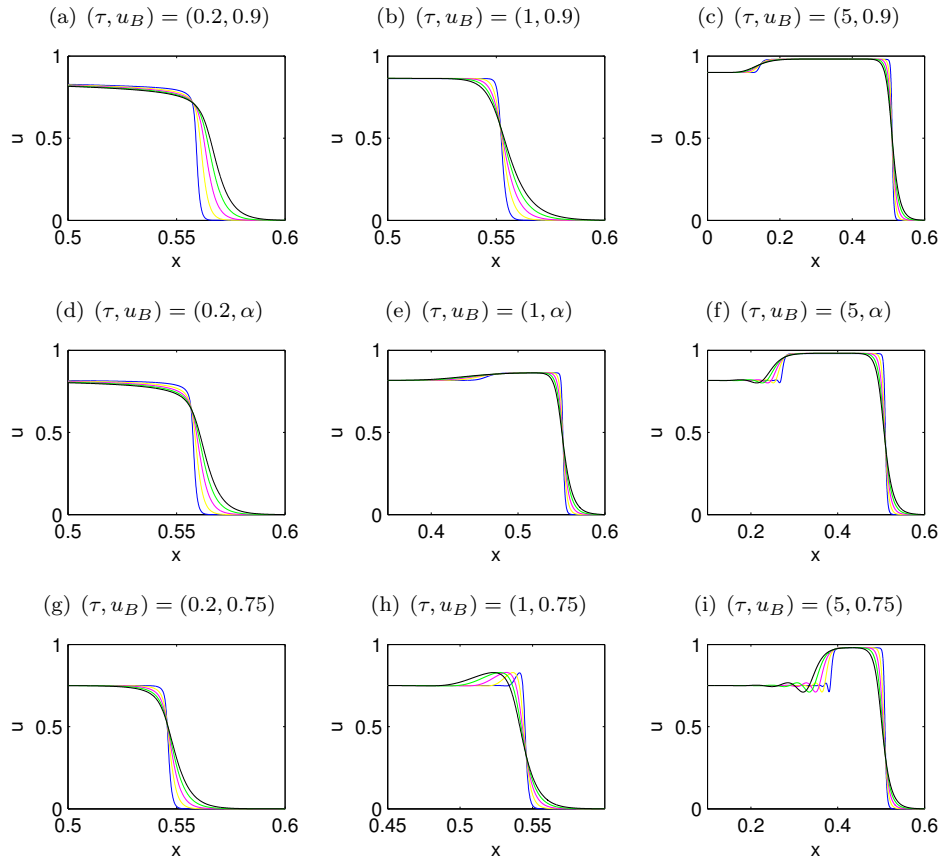


FIGURE 4.9. The numerical solutions of MBL equation at $T = 0.5$ with $\epsilon = 0.001$ (blue), $\epsilon = 0.002$ (yellow), $\epsilon = 0.003$ (magenta), $\epsilon = 0.004$ (green), and $\epsilon = 0.005$ (black). The view windows are zoomed into the regions where different ϵ values impose different solution profiles. The results are discussed in example 11.

525

5. CONCLUSION

526 We proved that the solution to the infinite domain problem can be approximated
 527 by that of the bounded domain problem. This provides a theoretical justification
 528 for using finite domain to calculate the numerical solution of the MBL equation
 529 (1.10). We also extended the classical central scheme originally designed for the
 530 hyperbolic systems to solve the MBL equation, which is of pseudo-parabolic type.
 531 The numerical solutions for qualitatively different parameter values τ and initial
 532 conditions u_B show that the jump locations are consistent with the theoretical
 533 calculation and the plateau heights are consistent with the numerically obtained
 534 values given in [21]. In particular, when $\tau > \tau_*$, for $u_B \in (\underline{u}, \bar{u})$, the numerical
 535 solutions give non-monotone water saturation profiles, which is consistent with the
 536 experimental observations. In addition, the order tests show that the proposed
 537 second and third order central schemes achieved the desired accuracies.

538 In [22, 20], the two-dimensional space extension of the modified Buckley-Leverett
 539 equation has been derived. One of the future directions is to develop high order
 540 numerical schemes to solve the two-dimensional MBL equation. Central schemes
 541 have been used to solve high dimensional hyperbolic problem and dispersive prob-
 542 lem ([11, 16]), which makes it a good candidate for such a task.

543 APPENDIX A. PROOF OF THE LEMMAS

544 *Proof to lemma 2.2.* Let $g(u) = \frac{f(u)}{u} = \frac{u}{u^2 + M(1-u)^2}$, then

$$g'(u) = \frac{M - (1+M)u^2}{(u^2 + M(1-u)^2)^2} \begin{cases} > 0 & \text{if } 0 < u < \sqrt{\frac{M}{M+1}} \\ = 0 & \text{if } u = \sqrt{\frac{M}{M+1}} \\ < 0 & \text{if } u > \sqrt{\frac{M}{M+1}} \end{cases}$$

545 and hence $g(u)$ achieves its maximum at $u = \sqrt{\frac{M}{M+1}}$. Therefore, $\frac{f(u)}{u} = g(u) \leq D$,
 546 where $D = \frac{f(\alpha)}{\alpha}$ and $\alpha = \sqrt{\frac{M}{M+1}}$, and in turn, we have that $f(u) \leq Du$ for all
 547 $0 \leq u \leq 1$. \square

Proof to lemma 2.3 (i).

$$\int_0^{+\infty} \left| e^{-\frac{x+\xi}{\epsilon\sqrt{\tau}}} - e^{-\frac{|x-\xi|}{\epsilon\sqrt{\tau}}} \right| e^{\frac{\lambda x - \lambda \xi}{\epsilon\sqrt{\tau}}} d\xi = \epsilon\sqrt{\tau} \frac{-2 + 2e^{\frac{(\lambda-1)x}{\epsilon\sqrt{\tau}}}}{\lambda^2 - 1} \leq \frac{2\epsilon\sqrt{\tau}}{1 - \lambda^2} \quad \text{if } \lambda \in (0, 1).$$

548 \square

Proof to lemma 2.3 (ii).

$$\int_0^{+\infty} \left| e^{-\frac{x+\xi}{\epsilon\sqrt{\tau}}} - e^{-\frac{|x-\xi|}{\epsilon\sqrt{\tau}}} \right| e^{\frac{\lambda x - \xi}{\epsilon\sqrt{\tau}}} d\xi = x e^{\frac{(\lambda-1)x}{\epsilon\sqrt{\tau}}} \leq \frac{\epsilon\sqrt{\tau}}{e(1-\lambda)} \quad \text{if } \lambda \in (0, 1).$$

549 \square

550 *Proof to lemma 2.3 (iii).* Based on the assumption on u_0 in (2.27)

$$(A.1) \quad \int_0^{+\infty} \left| e^{-\frac{x+\xi}{\epsilon\sqrt{\tau}}} - e^{-\frac{|x-\xi|}{\epsilon\sqrt{\tau}}} \right| e^{\frac{\lambda x}{\epsilon\sqrt{\tau}}} |u_0(\xi)| d\xi \leq \int_0^{+\infty} e^{-\frac{|x-\xi|}{\epsilon\sqrt{\tau}}} e^{\frac{\lambda x}{\epsilon\sqrt{\tau}}} |u_0(\xi)| d\xi \\ \leq C_u e^{\frac{\lambda x}{\epsilon\sqrt{\tau}}} \int_0^{L_0} e^{-\frac{|x-\xi|}{\epsilon\sqrt{\tau}}} d\xi = C_u y_1(x)$$

551 Calculating $y_1(x)$ with the assumption that $\lambda \in (0, 1)$, we get

$$y_1(x) = \begin{cases} e^{\frac{\lambda x}{\epsilon\sqrt{\tau}}} \int_0^{L_0} e^{-\frac{|x-\xi|}{\epsilon\sqrt{\tau}}} d\xi \leq 2\epsilon\sqrt{\tau} e^{\frac{\lambda x}{\epsilon\sqrt{\tau}}} \leq 2\epsilon\sqrt{\tau} e^{\frac{\lambda L_0}{\epsilon\sqrt{\tau}}} & \text{for } x \in [0, L_0] \\ e^{\frac{(\lambda-1)x}{\epsilon\sqrt{\tau}}} \int_0^{L_0} e^{\frac{\xi}{\epsilon\sqrt{\tau}}} d\xi \leq \epsilon\sqrt{\tau} e^{\frac{(\lambda-1)x + L_0}{\epsilon\sqrt{\tau}}} \leq \epsilon\sqrt{\tau} e^{\frac{\lambda L_0}{\epsilon\sqrt{\tau}}} & \text{for } x \in [L_0, +\infty) \end{cases}$$

552 Therefore, we get the desired inequality

$$\int_0^{+\infty} \left| e^{-\frac{x+\xi}{\epsilon\sqrt{\tau}}} - e^{-\frac{|x-\xi|}{\epsilon\sqrt{\tau}}} \right| e^{\frac{\lambda x}{\epsilon\sqrt{\tau}}} |u_0(\xi)| d\xi \leq 2C_u \epsilon\sqrt{\tau} e^{\frac{\lambda L_0}{\epsilon\sqrt{\tau}}}.$$

553 \square

554 *Proof to lemma 2.4 (i).*

555

$$\begin{aligned} & \int_0^{+\infty} \left| e^{-\frac{x+\xi}{\epsilon\sqrt{\tau}}} + \operatorname{sgn}(x-\xi)e^{-\frac{|x-\xi|}{\epsilon\sqrt{\tau}}} \right| e^{\frac{\lambda x - \lambda\xi}{\epsilon\sqrt{\tau}}} d\xi \\ &= \frac{\epsilon\sqrt{\tau}}{\lambda^2 - 1} \left(-2 + 2\lambda e^{\frac{(\lambda-1)x}{\epsilon\sqrt{\tau}}} - 2(\lambda-1)e^{-\frac{2x}{\epsilon\sqrt{\tau}}} \right) \leq \frac{2\epsilon\sqrt{\tau}}{1-\lambda^2} \quad \text{if } \lambda \in (0, 1). \end{aligned}$$

556

□

557 *Proof to lemma 2.4 (ii).*

558

$$\begin{aligned} & \int_0^{+\infty} \left| e^{-\frac{x+\xi}{\epsilon\sqrt{\tau}}} + \operatorname{sgn}(x-\xi)e^{-\frac{|x-\xi|}{\epsilon\sqrt{\tau}}} \right| e^{\frac{\lambda x - \xi}{\epsilon\sqrt{\tau}}} d\xi \\ &= \frac{2e^{\frac{(\lambda-3)x}{\epsilon\sqrt{\tau}}} - 2e^{\frac{(\lambda-1)x}{\epsilon\sqrt{\tau}}}}{\frac{-2}{\epsilon\sqrt{\tau}}} + xe^{\frac{(\lambda-1)x}{\epsilon\sqrt{\tau}}} \leq \epsilon\sqrt{\tau} + \frac{\epsilon\sqrt{\tau}}{e(1-\lambda)} \quad \text{if } \lambda \in (0, 1). \end{aligned}$$

559

□

560 *Proof to lemma 2.4 (iii).* Based on the assumption on u_0 in (2.27)

$$\begin{aligned} & \int_0^{+\infty} \left| e^{-\frac{x+\xi}{\epsilon\sqrt{\tau}}} + \operatorname{sgn}(x-\xi)e^{-\frac{|x-\xi|}{\epsilon\sqrt{\tau}}} \right| e^{\frac{\lambda x}{\epsilon\sqrt{\tau}}} |u_0(\xi)| d\xi \\ \text{(A.2)} \quad & \leq C_u e^{\frac{\lambda x}{\epsilon\sqrt{\tau}}} \int_0^{L_0} \left| e^{-\frac{x+\xi}{\epsilon\sqrt{\tau}}} + \operatorname{sgn}(x-\xi)e^{-\frac{|x-\xi|}{\epsilon\sqrt{\tau}}} \right| d\xi \\ & = C_u y_3(x) \end{aligned}$$

561 Calculating $y_3(x)$ with the assumption that $\lambda \in (0, 1)$, we get for $x \in [0, L_0]$

$$y_3(x) \leq e^{\frac{(\lambda-1)x}{\epsilon\sqrt{\tau}}} \int_0^x (e^{-\frac{\xi}{\epsilon\sqrt{\tau}}} + e^{\frac{\xi}{\epsilon\sqrt{\tau}}}) d\xi + e^{\frac{(\lambda+1)x}{\epsilon\sqrt{\tau}}} \int_x^{L_0} e^{-\frac{\xi}{\epsilon\sqrt{\tau}}} d\xi \leq 2\epsilon\sqrt{\tau} e^{\frac{\lambda L_0}{\epsilon\sqrt{\tau}}}$$

562 and

$$y_3(x) \leq e^{\frac{(\lambda-1)x}{\epsilon\sqrt{\tau}}} \int_0^{L_0} (e^{-\frac{\xi}{\epsilon\sqrt{\tau}}} + e^{\frac{\xi}{\epsilon\sqrt{\tau}}}) d\xi \leq \epsilon\sqrt{\tau} e^{\frac{(\lambda-1)x+L_0}{\epsilon\sqrt{\tau}}} \leq \epsilon\sqrt{\tau} e^{\frac{\lambda L_0}{\epsilon\sqrt{\tau}}}$$

563 for $x \in [L_0, +\infty)$.

564 Therefore, we get the desired inequality

$$\int_0^{+\infty} \left| e^{-\frac{x+\xi}{\epsilon\sqrt{\tau}}} + \operatorname{sgn}(x-\xi)e^{-\frac{|x-\xi|}{\epsilon\sqrt{\tau}}} \right| e^{\frac{\lambda x}{\epsilon\sqrt{\tau}}} |u_0(\xi)| d\xi \leq 2C_u \epsilon\sqrt{\tau} e^{\frac{\lambda L_0}{\epsilon\sqrt{\tau}}}.$$

565

□

Proof to lemma 2.5 (i).

$$\left| \phi_1(x) - e^{-\frac{x}{\epsilon\sqrt{\tau}}} \right| = e^{-\frac{L}{\epsilon\sqrt{\tau}}} \left| \frac{e^{-\frac{x}{\epsilon\sqrt{\tau}}} - e^{\frac{x}{\epsilon\sqrt{\tau}}}}{e^{\frac{L}{\epsilon\sqrt{\tau}}} - e^{-\frac{L}{\epsilon\sqrt{\tau}}}} \right| = e^{-\frac{L}{\epsilon\sqrt{\tau}}} |\phi_2(x)|.$$

566

□

567 *Proof to lemma 2.5 (ii).* Since $\phi_2(x) = \frac{e^{\frac{x}{\epsilon\sqrt{\tau}}} - e^{-\frac{x}{\epsilon\sqrt{\tau}}}}{e^{\frac{L}{\epsilon\sqrt{\tau}}} - e^{-\frac{L}{\epsilon\sqrt{\tau}}}}$, we see that $\phi_2'(x) = \frac{1}{\epsilon\sqrt{\tau}} \frac{e^{\frac{x}{\epsilon\sqrt{\tau}}} + e^{-\frac{x}{\epsilon\sqrt{\tau}}}}{e^{\frac{L}{\epsilon\sqrt{\tau}}} - e^{-\frac{L}{\epsilon\sqrt{\tau}}}} >$
 568 0 and hence $\phi_2(x) \leq \phi_2(L) = 1$ for $x \in [0, L]$. □

569 *Proof to lemma 2.5 (iii).* $\phi'_2(x) = \frac{1}{\epsilon\sqrt{\tau}} \frac{e^{\frac{x}{\epsilon\sqrt{\tau}}} + e^{-\frac{x}{\epsilon\sqrt{\tau}}}}{\frac{L}{\epsilon\sqrt{\tau}} - e^{-\frac{L}{\epsilon\sqrt{\tau}}}}$ gives that $\phi''_2(x) = \frac{1}{\epsilon^2\tau} \phi_2(x) >$
 570 0 , and hence $\phi'_2(x) \leq \phi'_2(L) = \frac{1}{\epsilon\sqrt{\tau}} \frac{e^{\frac{L}{\epsilon\sqrt{\tau}}} + e^{-\frac{L}{\epsilon\sqrt{\tau}}}}{\frac{L}{\epsilon\sqrt{\tau}} - e^{-\frac{L}{\epsilon\sqrt{\tau}}}} = \frac{1}{\epsilon\sqrt{\tau}} \frac{e^{\frac{2L}{\epsilon\sqrt{\tau}}} + 1}{e^{\frac{2L}{\epsilon\sqrt{\tau}}} - 1} \leq \frac{2}{\epsilon\sqrt{\tau}}$ if $\epsilon \ll 1$ for
 571 $x \in [0, L]$. □

572

ACKNOWLEDGMENTS

573 CYK would like to thank Prof. L.A. Peletier for introducing MBL equation and
 574 Mathematical Biosciences Institute at OSU for the hospitality and support.

575

REFERENCES

- 576 [1] J. L. Bona, H.-Q. Chen, S. M. Sun, and B.-Y. Zhang, *Comparison of quarter-plane and two-*
 577 *point boundary value problems: the BBM-equation*, Discrete Contin. Dyn. Syst. **13** (2005),
 578 no. 4, 921–940. MR MR2166711 (2006m:35314)
- 579 [2] J. L. Bona and L.-H. Luo, *Initial-boundary value problems for model equations for the prop-*
 580 *agation of long waves*, Evolution equations (Baton Rouge, LA, 1992), Lecture Notes in
 581 Pure and Appl. Math., vol. 168, Dekker, New York, 1995, pp. 63, 65–94. MR MR1300420
 582 (95i:35137)
- 583 [3] S.E. Buckley and M.C. Leverett, *Mechanism of fluid displacement in sands*, Petroleum Trans-
 584 actions, AIME **146** (1942), 107–116.
- 585 [4] B. Cockburn, C. Johnson, C.-W. Shu, and E. Tadmor, *Advanced numerical approximation*
 586 *of nonlinear hyperbolic equations*, Lecture Notes in Mathematics, vol. 1697, Springer-Verlag,
 587 Berlin, 1998, Papers from the C.I.M.E. Summer School held in Cetraro, June 23–28, 1997,
 588 Edited by Alfio Quarteroni, Fondazione C.I.M.E.. [C.I.M.E. Foundation]. MR MR1729305
 589 (2000h:65004)
- 590 [5] B. Cockburn, G. E. Karniadakis, and C-W (Eds.) Shu, *Discontinuous galerkin methods: The-*
 591 *ory, computation and applications*, Lecture Notes in Computational Science and Engineering,
 592 2000.
- 593 [6] A.T. Corey, *The interrelation between gas and oil relative permeabilities*, Producer’s Monthly
 594 **19** (1954), no. 1, 38–41.
- 595 [7] D. A. DiCarlo, *Experimental measurements of saturation overshoot on infiltration*, Water
 596 Resources Research **40** (2004), 4215.1 – 4215.9.
- 597 [8] S.M Hassanizadeh and W.G. Gray, *Mechanics and thermodynamics of multiphase flow in*
 598 *porous media including interphase boundaries*, Adv. Water Resour. **13** (1990), 169–186.
- 599 [9] ———, *Thermodynamic basis of capillary pressure in porous media*, Water Resour. Res. **29**
 600 (1993), 3389–3405.
- 601 [10] H. Hugoniot, *Propagation des Mouvements dans les Corps et specialement dans les Gaz*
 602 *Parfaits (in French)*, Journal de l’Ecole Polytechnique **57** (1887), 3–97.
- 603 [11] G-S Jiang and E. Tadmor, *Nonoscillatory central schemes for multidimensional hyper-*
 604 *bolic conservation laws*, SIAM J. Sci. Comput. **19** (1998), no. 6, 1892–1917 (electronic).
 605 MR 1638064 (99f:65128)
- 606 [12] A. Kurganov and D. Levy, *A third-order semidiscrete central scheme for conservation laws*
 607 *and convection-diffusion equations*, SIAM J. Sci. Comput. **22** (2000), no. 4, 1461–1488 (elec-
 608 tronic). MR MR1797891 (2001j:65127)
- 609 [13] A. Kurganov and C.-T. Lin, *On the reduction of numerical dissipation in central-upwind*
 610 *schemes*, Commun. Comput. Phys. **2** (2007), no. 1, 141–163. MR MR2305919 (2007k:35320)
- 611 [14] R. J. LeVeque, *Numerical methods for conservation laws*, second ed., Lectures in Mathematics
 612 ETH Zürich, Birkhäuser Verlag, Basel, 1992. MR MR1153252 (92m:65106)
- 613 [15] ———, *Finite volume methods for hyperbolic problems*, Cambridge Texts in Applied Math-
 614 ematics, Cambridge University Press, Cambridge, 2002. MR MR1925043 (2003h:65001)
- 615 [16] D. Levy, G. Puppo, and G. Russo, *Compact central WENO schemes for multidimen-*
 616 *sional conservation laws*, SIAM J. Sci. Comput. **22** (2000), no. 2, 656–672. MR 1780619
 617 (2001d:65110)
- 618 [17] W. J. Macquorn Rankine, *On the thermodynamic theory of waves of finite longitudinal dis-*
 619 *turbance*, Royal Society of London Philosophical Transactions Series I **160** (1870), 277–288.

- 620 [18] H. Nessyahu and E. Tadmor, *Nonoscillatory central differencing for hyperbolic conservation*
621 *laws*, J. Comput. Phys. **87** (1990), no. 2, 408–463. MR MR1047564 (91i:65157)
- 622 [19] O. A. Oleĭnik, *Discontinuous solutions of non-linear differential equations*, Uspehi Mat. Nauk
623 (N.S.) **12** (1957), no. 3(75), 3–73. MR MR0094541 (20 #1055)
- 624 [20] C. J. Van Duijn, A. Mikelic, and I.S. Pop, *Effective Buckley-Leverett equations by homoge-*
625 *nization*, Progress in industrial mathematics at ECMI (2000), 42–52.
- 626 [21] C. J. van Duijn, L. A. Peletier, and I. S. Pop, *A new class of entropy solutions of the*
627 *Buckley-Leverett equation*, SIAM J. Math. Anal. **39** (2007), no. 2, 507–536 (electronic).
628 MR MR2338418 (2008g:35136)
- 629 [22] Y. Wang, *Central schemes for the modified buckley-leverett equation*, Ph.D. thesis, The Ohio
630 State University, 2010.
- 631 [23] Y. Xu and C-W. Shu, *A local discontinuous Galerkin method for the Camassa-Holm equation*,
632 SIAM J. Numer. Anal. **46** (2008), no. 4, 1998–2021. MR MR2399405 (2009e:65140)
- 633 [24] ———, *Local discontinuous Galerkin method for the Hunter-Saxton equation and its zero-*
634 *viscosity and zero-dispersion limits*, SIAM J. Sci. Comput. **31** (2008/09), no. 2, 1249–1268.
635 MR MR2466156 (2009k:65187)

636 DEPARTMENT OF MATHEMATICS, THE OHIO STATE UNIVERSITY, 231 WEST 18TH AVE, COLUM-
637 BUS, OH 43210

638 *Current address:* School of Mathematics, University of Minnesota, 127 Vincent Hall 206 Church
639 St SE, Minneapolis, MN 55455

640 *E-mail address:* wang@math.umn.edu

641 DEPARTMENT OF MATHEMATICS, THE OHIO STATE UNIVERSITY, 231 WEST 18TH AVE, COLUM-
642 BUS, OH 43210; MATHEMATICAL BIOSCIENCES INSTITUTE, THE OHIO STATE UNIVERSITY, 1735
643 NEIL AVE, COLUMBUS, OH 43210

644 *E-mail address:* kao@math.ohio-state.edu